Fall 2020

Constructing a Time Scale of Biotic Recovery Across the Cretaceous–Paleogene Boundary, Corral Bluffs, Denver Basin, Colorado, U.S.A.

Vincent Isakson
Boise State University

Mark D. Schmitz
Boise State University

For a complete list of authors, please see the article.

Constructing a time scale of biotic recovery across the Cretaceous–Paleogene boundary, Corral Bluffs, Denver Basin, Colorado, U.S.A.

Anthony J. Fuentes[1]*, **William C. Clyde[1]**, **Ken Weissenburger[2]**, **Antoine Bercovici[3]**, **Tyler R. Lyson[2]**, **Ian M. Miller[2]**, **Jahandar Ramezani[4]**, **Vincent Isakson[5]**, **Mark D. Schmitz[5]**, and **Kirk R. Johnson[3]**

[1]*Department of Earth Sciences, University of New Hampshire, 56 College Rd., Durham, NH 03824, U.S.A.*

[2]*Department of Earth Sciences, Denver Museum of Nature & Science, 2001 Colorado Blvd., Denver, CO 80205, U.S.A.*

[3]*Department of Paleobiology, MRC-121, National Museum of Natural History, Smithsonian Institution, 10th St. and Constitution Ave. NW, Washington, D.C. 20560-0121, U.S.A.*

[4]*Department of Earth, Atmospheric, and Planetary Sciences, Massachusetts Institute of Technology, Green Building, 77 Massachusetts Ave., Cambridge, MA 02139, U.S.A.*

[5]*Department of Geosciences, Boise State University, 1910 University Dr., Boise, ID 83725-1535, U.S.A.*

*Correspondence should be addressed to: anthonyjosephfuentes@gmail.com

ABSTRACT

The Cretaceous–Paleogene (K–Pg) boundary interval represents one of the most significant mass extinctions and ensuing biotic recoveries in Earth history. Earliest Paleocene fossil mammal faunas corresponding to the Puercan North American Land Mammal Age (NALMA) are thought to be highly endemic and potentially diachronous, necessitating precise chronostratigraphic controls at key fossil localities to constrain recovery dynamics in continental biotas following the K–Pg mass extinction. The Laramide synorgenic sedimentary deposits within the Denver Basin in east-central Colorado preserve one of the most continuous and fossiliferous records of the K–Pg boundary interval in North America. Poor exposure in much of the Denver Basin, however, makes it difficult to correlate between outcrops. To constrain fossil localities in coeval strata across the basin, previous studies have relied upon chronostratigraphic methods such as magnetostratigraphy. Here, we present a new high-resolution magnetostratigraphy of 10 lithostratigraphic sections spanning the K–Pg boundary interval at Corral Bluffs located east of Colorado Springs in the southern part of the Denver Basin. Fossil localities from Corral Bluffs have yielded limited dinosaur remains, mammal fossils assigned to the Puercan NALMA, and numerous fossil leaf localities. Palynological analyses identifying the K–Pg boundary in three sections and two independent, but nearly identical, $^{206}Pb/^{238}U$ age estimates for the same volcanic ash, provide key temporal calibration points. Our paleomagnetic analyses have identified clear polarity reversal boundaries from chron C30n to chron C28r across the sections. It is now possible to place the fossil localities at Corral Bluffs within the broader basin-wide chronostratigraphic framework and evaluate them in the context of K–Pg boundary extinction and recovery.

KEY WORDS: Corral Bluffs, Cretaceous, D1 sequence, Denver Basin, K–Pg boundary, magnetostratigraphy, Paleocene, Paleogene, Puercan North American Land Mammal Age, U–Pb geochronology.

INTRODUCTION

The Cretaceous–Paleogene (K–Pg) boundary is associated with one of the most significant periods of biological turnover in Earth history. It corresponds to one of the three largest mass extinctions and is followed by a profound adaptive radiation of modern taxa, most notably mammals, in the Paleocene (Schulte et al., 2010; Halliday et al., 2017). Whereas the drivers and signature of the K–Pg mass extinction is the subject of active and extensive discussion in the literature (Alvarez et al., 1980; Courtillot et al., 1986; Schulte et al., 2010; Schoene et al., 2015, 2019; Sprain et al., 2019), the recovery dynamics in the subsequent earliest Paleocene have received much less attention. A more comprehensive understanding of the recovery after the rapid and catastrophic end-Cretaceous mass extinction may provide insights into how the modern biosphere will respond to the ongoing anthropogenic-driven extinction event.

Numerous vertebrate fossil localities spanning the Late Cretaceous to Paleocene have been identified within western North American inte-

Anthony J. Fuentes, William C. Clyde, Ken Weissenburger, Antoine Bercovici, Tyler R. Lyson, Ian M. Miller, Jahandar Ramezani, Vincent Isakson, Mark D. Schmitz, and Kirk R. Johnson

rior basins (e.g., Williamson, 1996; Eberle and Lillegraven, 1998; Clemens, 2002; Hunter and Archibald, 2002; Eberle, 2003; Lofgren et al., 2004; Middleton and Dewar., 2004; Wilson, 2013). The mammalian faunas comprising the Puercan North American Land Mammal Age (NALMA) are especially significant as this interval coincides with the onset of biotic recovery immediately following the K–Pg mass extinction (Lofgren et al., 2004). While the North American Western Interior includes the best record of early Paleocene mammalian fossil localities in the world, the total number of localities and overall availability of fossil material remains limited. The identification of new localities and continued sampling of existing localities are critical to isolating the factors driving the recovery following the K–Pg mass extinction; moreover, temporal constraints provided by high-resolution chronostratigraphic studies are critical to pace the recovery within continental strata. Puercan mammalian faunas are highly endemic making it difficult to identify biostratigraphic patterns across the region, further necessitating the use of chronostratigraphic methods that are independent of biostratigraphy to properly deconvolve the regional scale drivers of recovery (Lofgren et al., 2004). Magnetostratigraphy is commonly and effectively used for this purpose. This method correlates an observed pattern of paleomagnetic polarity reversals in a stratigraphic sequence to the independently dated geomagnetic polarity time scale (GPTS) (Gradstein et al., 2012; Ogg, 2012), thereby constraining a stratigraphic section to a well-calibrated time interval.

The Laramide synorgenic sediment sequence within the Denver Basin represents one of the best terrestrial records of the K–Pg boundary in the world with observed osmium and iridium anomalies, shocked quartz, extinction of flora and fauna, and a spike in abundance of fern spores that are commonly used as indicators of the boundary (Nichols and Fleming, 2002; Barclay, 2003; Raynolds and Johnson, 2003; Zaiss et al., 2014). Several important megafloral and vertebrate paleontological localities have been identified within the basin; however, the Denver Basin is relatively under-sampled in comparison to coeval sites in the San Juan Basin of New Mexico and the Williston Basin of North Dakota and Montana (Archibald, 1982; Williamson, 1996; Clemens, 2002; Williamson et al., 2012; Wilson, 2013; Smith et al., 2018). There are 231 Puercan-aged mammal localities globally recorded in the Paleobiology Database, 185 of which are in the greater Rocky Mountain region of North America. Of these sites, 101 are from New Mexico, North Dakota, and Montana (Paleobiology Database, 2019).

Previous discoveries of an in-situ Paleocene rainforest at Castle Rock and the relatively high mammalian diversity of the Littleton fauna, both in the Denver Basin, allude to the incredible potential this region has in yielding informative fossil material to help elucidate the post-K–Pg extinction recovery dynamics within the central North American Western Interior (Johnson and Ellis, 2002; Ellis et al., 2003; Middleton and Dewar., 2004; Dahlberg et al., 2016). A barrier to developing a coherent stratigraphic framework for existing and new fossil localities in the Denver Basin is the disparate nature of exposure, which makes it difficult to tie localities to one another via lithostratigraphy. Fortunately, magnetostratigraphy calibrated through palynology and radiometric ages can surmount this barrier and provide an independent chronology of biologic turnover in the Denver Basin that can be compared to other basins.

Much of the previous paleontological and chronostratigraphic work in the Denver Basin has been focused in the central portion of the basin in and around Denver, highlighting the need for more detailed, expansive prospecting, and stratigraphic correlation in other parts of the basin (Hicks et al., 2003; Clyde et al., 2016). Previous studies have identified Late Cretaceous through Paleocene fossil leaf localities and Puercan mammal localities at the Jimmy Camp Creek and Corral Bluffs field site (hereafter referred to as "Corral Bluffs"), located east of Colorado Springs in the southernmost part of the basin (Johnson et al., 2003; Eberle, 2003). This study presents a high-resolution chronostratigraphy for Corral Bluffs that allows existing and future Late Cretaceous–early Paleocene fossil localities to be placed in a precise temporal context (Figs. 1A–B). This is achieved through compiling a magnetostratigraphic framework calibrated by uranium–lead (U–Pb) geochronology and a palynologically defined K–Pg boundary. This new chronology for Corral Bluffs will allow the lithostratigraphic units and associated fossil localities within this field area to be tied into the broader basin-wide chronostratigraphic framework, which will ultimately help better constrain the timing and drivers of the post-K–Pg extinction recovery in this region.

Extinction and Recovery across the K–Pg Boundary

Mass extinctions are typified by an initial catastrophic loss of taxa followed by a low-diversity "recovery" interval dominated by surviving taxa (Erwin, 2001; Hull et al., 2015). The detailed patterns of biotic recovery following the K–Pg mass extinction, however, are complicated and subject to regional biogeographic and taxonomic variability. For example, there is ongoing debate as to whether distance from the Chicxulub impact site in southern Mexico's Yucatan Peninsula can serve as proxy for the severity and timing of biotic recovery across the K–Pg boundary (Witts et al., 2016; Lowery et al., 2018). Consistent with this idea are numerous studies of paleofloral assemblages suggesting that North America, which is relatively close to the Chicxulub impact site, experienced higher rates of extinction, and delayed recovery, compared to southern hemisphere sites (Erwin, 2001; Nichols and Fleming, 2002; Iglesias et al., 2007; Clyde et al., 2014). However, a recent study of the diversity of benthic marine organisms within the Chicxulub crater itself

concluded that biologic productivity and diversity had recovered within 30 thousand years (k.y.), in contrast to sites in other parts of the Gulf of Mexico that took 300 k.y. or more to return to pre-impact levels (Lowery et al., 2018). Such heterogeneous patterns of K–Pg extinction and recovery have been documented for numerous other taxonomic groups and biogeographic regions, suggesting that this is more the rule than the exception (Jablonski, 1998; Håkansson and Thomsen, 1999; Kiessling and Baron-Szabo, 2004; Vajda and McLoughlin, 2007; Hull and Norris, 2011; Mizukami et al., 2013; Vajda and Bercovici, 2014; Witts et al., 2016; Donovan et al., 2018).

Floras of the Late Cretaceous are largely dominated by angiosperms, and the K–Pg boundary in the North American Western Interior is associated with an ~57–78% loss of plant diversity (Johnson, 2002) as well as an ~33% extinction in the pollen record (Nichols and Johnson, 2002). The immediate recovery is characterized by the fern spike interval representing the first few thousand years after the bolide impact during which pioneer plants recolonize the devastated landscape, followed by a low-diversity interval dominated by dicotyledonous angiosperms (Johnson, 2002; Barclay, 2003; Vajda and Bercovici, 2014; Clyde et al. 2016; Fastovsky and Bercovici, 2016). Regional heterogeneity is also observed in the vegetation of the Western Interior as localities in Saskatchewan, Canada, record a mass kill of standing vegetation, but no clear evidence of mass extinction of paleoflora (McIver, 1999; Johnson and Ellis, 2002; Vajda and McLoughlin, 2007); whereas, the palynological record shows a similar signature to that of the Western Interior (Sweet et al., 1990, 1999; Sweet and Braman, 1992, 2001).

Despite ongoing debate as to the origination of crown placental mammals, the most important diversification of eutherian mammals seems to coincide with the K–Pg boundary (O'Leary et al., 2013; Grossnickle and Newham, 2016; Davies et al., 2017). The Western Interior presents the best-documented record of the K–Pg extinction on land with the highest density of vertebrate fossil localities spanning the boundary (Clemens, 2002). As noted for other groups, the recovery dynamics of mammals from the Western Interior are heterogenous as the speed and severity of turnover at the K–Pg boundary vary depending on the spatiotemporal resolution of the study (Wilson, 2013; Longrich et al., 2016; Close et al., 2019). In general, however, rapid and severe declines in mammalian taxonomic diversity are reported across North America during this interval (Wilson, 2014; Longrich et al., 2016). Mammalian taxa with more widely spread geographic ranges and morphologies corresponding to an omnivorous feeding mode are associated with a higher likelihood of crossing the K–Pg boundary (Wilson, 2013; Longrich et al., 2016).

Pu1 (*Protongulatum/Ectoconus* Interval Zone) is characterized primarily by low ecological and morphological diversity in the Western Interior, mirroring the diversity trends of the paleoflora (Wilson, 2014). Opportunistic immigrant taxa spearheaded by archaic ungulates are common in the earliest Paleocene, possibly from refugia either to the north or south of the Western Interior (Lofgren et al., 2004; Wilson, 2014). Assemblages from the Hell Creek region of northwest Montana indicate that recovery of mammal communities in this area took between 320 k.y. and 1 million years (m.y.) with eutherian taxa taking 400 k.y. to 1 m.y. to recover (Wilson, 2014; Smith et al., 2018). Lillegraven and Eberle (1999) noted that the eutherian faunas in the Ferris Formation of south-central Wyoming's Hanna Basin do not show significant losses at the K–Pg boundary, but instead radiate to fill vacant niche space. The onset of Pu2 (*Ectoconus/Taeniolabis taoensis* Interval Zone) has been noted to coincide with an increase in both body size and morphologic complexity of mammals, most notably the rapid diversification of archaic ungulates (Lillegraven and Eberle, 1999; Lofgren et al., 2004). Pu2 and the onset of Pu3 (*Taeniolabis taoensis/Periptychus carinidens* Interval Zone) coincide with increasing north to south provinciality of mammalian assemblages (Lofgren et al., 2004). The provinciality of Pu2 and Pu3 faunas is often confounded by stratigraphic concerns (e.g., reworking, incision by channels) at important localities, such as in the Hell Creek region of the Williston Basin (Lillegraven and Eberle, 1999; Clemens 2002; Lofgren et al., 2004). The Pu3 interval zone continues the diversity trends established during the Pu2 interval zone with considerable compositional overlap between the two interval zones (Eberle and Lillegraven, 1998). While details of the onset and tempo of initial recovery for North American mammals are still largely unresolved, by the Pu2–Pu3 transition, mammal communities had largely returned to pre-extinction levels of diversity across the Western Interior and began to expand rapidly into new available niche space (Eberle and Lillegraven 1998; Lillegraven and Eberle 1999; Wilson, 2014).

The global patterns and rates of extinction and recovery during and following the K–Pg mass extinction appear to be more stochastic than simply a function of proximity to the impact site. Recovery dynamics may instead be primarily governed by biotic factors like evolution of novel adaptations and immigration, and high-resolution temporal frameworks are needed to better understand the tempo and mode of these processes.

GEOLOGIC SETTING

The Denver Basin is a Laramide perimeter basin located primarily in central and eastern Colorado to the east of the Front Range, which defines the western boundary of the basin (Raynolds, 2002). Outcrops in the Denver Basin are difficult to correlate lithostratigraphically due to the low-relief and poor exposure throughout the basin; thus, other chronostratigraphic methods have been relied
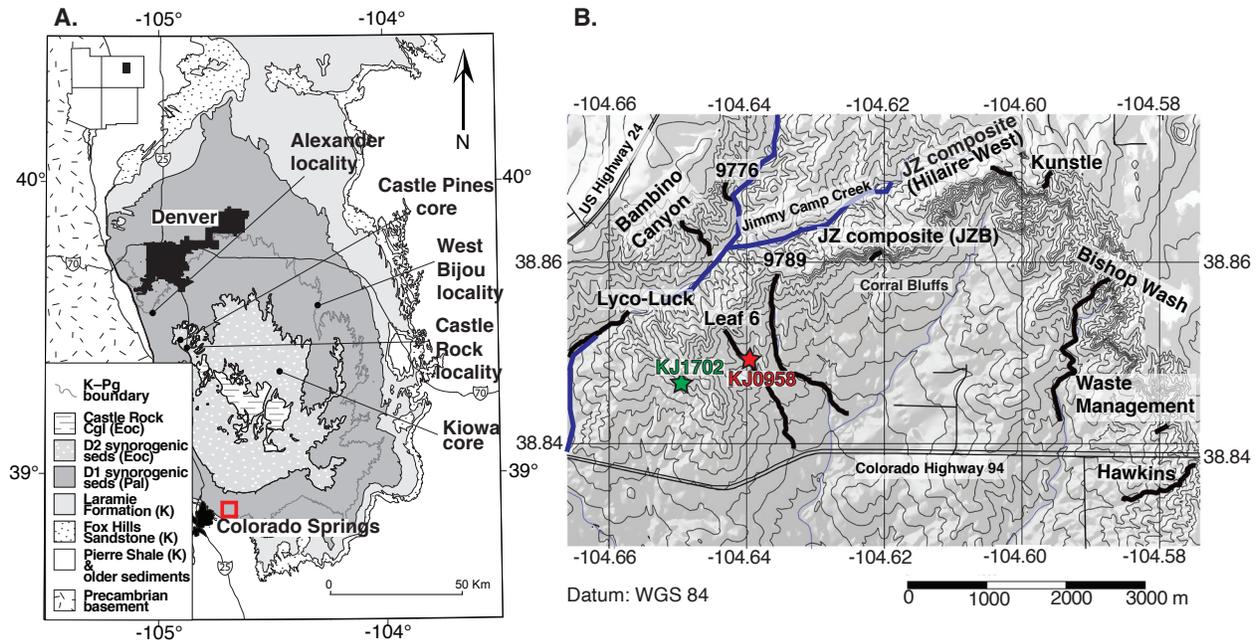
Anthony J. Fuentes, William C. Clyde, Ken Weissenburger, Antoine Bercovici, Tyler R. Lyson, Ian M. Miller, Jahandar Ramezani, Vincent Isakson, Mark D. Schmitz, and Kirk R. Johnson

Figure 1. A, Geologic map of the Denver Basin, modified from Clyde et al. (2016), showing the locations of the Castle Pines and Kiowa cores in relation to the Corral Bluffs/Jimmy Camp Creek field site (red square). Positions of important fossil sites at the Alexander, West Bijou, and Castle Rock localities within the basin are shown. Abbreviations: Cgl = Conglomerate; Eoc = Eocene; K = Cretaceous; Pal = Paleocene; seds = sediments. **B,** Map of the Corral Bluffs/Jimmy Camp Creek field site showing the 10 stratigraphic sections studied here (black lines with large black text labels). Position of Jimmy Camp Creek area of field site shown by dark blue line with smaller black text. Corral Bluffs labeled to the southeast of Jimmy Camp Creek. The JZ composite section is composed of the JZB and Hilaire-West subsections. The map also shows the location of ash samples KJ0958 (red star and text) and KJ1702 (green star and text). The 10 sections include, from left, (1) Lyco-Luck; (2) Bambino Canyon; (3) Leaf 6; (4) 9776; (5) 9789; (6) JZ composite (which includes subsections JZB and Hilaire-West); (7) Kunstle; (8) Bishop Wash; (9) Waste Management; and (10) Hawkins.

upon to correlate between exposures (Hicks et al., 2003; Raynolds and Johnson, 2003; Clyde et al., 2016). In addition to information provided by surface outcrops, data from two drilling cores are also available to researchers. These include the Castle Pines and Kiowa cores, which span Upper Cretaceous- to Eocene-aged units (Fig. 1A). The more western and mountain-proximal Castle Pines core was drilled in 1987 near Castle Pines, Colorado, and the Kiowa core was drilled during 1999 in the central region of the Denver Basin within the town Kiowa, Colorado (Robson and Banta, 1993; Raynolds et al., 2001). While the two cores sampled the same units, the thicknesses of the cores (Castle Pines = 3,120 ft [~951 m]; Kiowa = 2,256 ft [~688 m]) are evidence of eastward distal thinning of the Denver Basin (Raynolds, 2002). This is likely a function of greater tectonic subsidence in the region adjacent to the uplift at the time of the deposition of the synorogenic sequences.

The Upper Cretaceous, pre-orogenic units in the Denver Basin are the Pierre Shale, Fox Hills Sandstone, and Laramie Formation and reflect the regression of the Western Interior Seaway (Raynolds, 2002; Fig. 1A this paper). The

Laramide synorogenic strata of the Denver Basin are divided into two sedimentary packages, the D1 and D2 sequences, separated unconformably by a distinctive paleosol (Farnham and Kraus, 2002; Raynolds, 2002). These sequences correspond to two distinct pulses of sedimentation coincident with uplift of the Front Range (Raynolds, 2002).

This study is located within the Upper Cretaceous to lower Paleocene D1 sequence of Raynolds, 2002 (Fig. 1A). This sequence is composed of fluvial/lacustrine sandstone, mudstone, and lignite beds underlain by the Upper Cretaceous Laramie Formation and unconformably overlain by the Eocene D2 sequence. The D1 sequence records the deposition of eroded material from the unroofing of the Front Range during the interval from 68 to 64 Ma (Wilson, 2002; Raynolds and Johnson, 2003). The compositions of the sediments within the D1 sequence correspond to the successive removal and deposition of Mesozoic and Paleozoic sedimentary cover, volcanic rocks, and Precambrian basement material mantling the Front Range during the Laramide uplift (Kelley, 2002; Raynolds, 2002; Wilson, 2002). The gradational transition from mountain-proximal alluvial facies to more distal fluvial and paludal facies is

indicative of a dynamic landscape associated with the active uplift and unroofing of the Front Range at this time.

The facies exposed within Corral Bluffs are indicative of a fluvial depositional environment with lithologies ranging from coarse channel sandstone, overbank mud and siltstone deposits, lignite, carbonaceous shale, and fine, muddy sandstone. The field site is characterized by stark changes in relief from flat plains with sparse-covered outcrops at the base of the cliffs at Corral Bluffs to steep, well-exposed cliffs within which most of the paleomagnetic sampling was completed. The outcrops within the plains at the base of the bluffs are less frequent and subject to greater variations in dip closer to the contact with the underlying Laramie Formation. Direct stratigraphic correlations between sections at Corral Bluffs are difficult due to extensive cover by quaternary alluvium and variable dips in the low-relief portion of the field area, laterally discontinuous beds, and isolated outcrops.

METHODS

Paleomagnetism

Field Sampling

We collected 548 oriented hand samples from 126 sites in 10 stratigraphic sections across the Corral Bluffs field area during the 2017 and 2018 field seasons, with a minimum of four samples taken from each site (Fig. 1B). Thirty-two samples from 10 previously unanalyzed sites from the Leaf 6 section collected during a 2009 field reconnaissance were also made available, for a total of 580 samples collected across 136 sites. Sampling was guided by the previous magnetostratigraphic work of Hicks et al. (2003), who identified polarity reversals corresponding to the C30n–C29r and C29r–C29n boundaries in their Jimmy Camp Creek section (our Lyco-Luck section) and their JZ section (our JZ composite section). Our sampling was limited to fine-grained lithologies such as mudstone, siltstone, and muddy, fine-grained sandstone (Supplement Table S1 [Table S1]). Approximately 0.5 m of overburden was removed before sampling to minimize the effects of modern weathering. Slumps and channels were avoided for sampling, although site CB1804 from the 9776 section was later determined to be sampled from slumped material and was not included in the final data table (Table S2).

A Differential Global Navigation Satellite System (DGNSS; Trimble® Juno T41 S model) was used to collect waypoints at each sample site, and these data were post-processed using a nearby Continuously Operating Reference Station. These DGNSS data were used in conjunction with hand levelling to determine stratigraphic levels within a section. Correlation between sections is challenging. Local lithologic controls are available from the 9789 section to the Bishop Wash section in the form of traceable sandstone bodies. The westernmost sections (Lyco-Luck, Bambino Canyon, Leaf 6, and 9776), however, are difficult to correlate lithostratigraphically due to low relief, variable dips, and large covered areas. To account for the heterogeneity in available lithostratigraphic tracers across the sections, elevation from the DGNSS measurements is used as the primary stratigraphic framework for this study (Tables S2–S3). Elevation error for DGNSS measurements like these is typically < 0.5 m, allowing for the superposition of nearly all the sample sites to be resolved correctly relative to field observations. In cases where the superposition of closely spaced sites was not properly resolved by DGNSS (i.e., because of steep overhanging cliffs causing poor Global Navigation Satellite System reception) or where we had clearly erroneous or missing DGNSS measurements, we estimated elevation values (signified by *italics* in Tables S2–S3). These estimated values were determined using hand levelling or interpolated using field notes and Google Earth to calculate the proportional elevation difference between two bracketing sites with definitive DGNSS values and the unknown site. The difference between the two bracketing DGNSS elevations was multiplied by the proportion calculated from the Google Earth analysis and added to the elevation of the lower sample to derive the estimated elevation for the unknown site. Site DB0902 was sampled from the same outcrop as CB1735, but during a different field season and was estimated to lie no more than 1 m below CB1735 (Table S2). Stratigraphic positions for CB1805 and CB1809 could not be estimated, because they are located in a subsidiary gully to the main Bambino Canyon section and, therefore, are not included in the magnetostratigraphic results. The estimated DGNSS-derived stratigraphic thickness of the Lyco-Luck section within Jimmy Camp Creek appears to be more compressed relative to the other sections probably due to its relatively long horizontal distance, small change in elevation, and relatively steep 3° dip.

We acknowledge that the stratigraphic thicknesses determined using DGNSS elevation are minimum estimates of true thicknesses; however, this method allows us to use a completely independent and objective frame of reference to identify shared polarity reversals across sections that could not be correlated lithostratigraphically due to outcrop cover. Also, dips in the field area are generally < 3° and difficult to measure accurately, so elevation serves as a reasonable proxy for stratigraphic level. Our identification and correlation of the paleomagnetic reversals at Corral Bluffs within an absolute elevation framework will allow for future work to more comprehensively model stratigraphic thicknesses using the chron boundaries as stratigraphic datums.

Laboratory Methods

Paleomagnetic hand samples were cut into 8 cm^3 cubes, retaining the oriented surface as one cube face, and analyzed at the University of New Hampshire Paleomagnetism Laboratory. Samples were measured using a 2G Enterprises superconducting quantum interference device (SQUID)

Anthony J. Fuentes, William C. Clyde, Ken Weissenburger, Antoine Bercovici, Tyler R. Lyson, Ian M. Miller, Jahandar Ramezani, Vincent Isakson, Mark D. Schmitz, and Kirk R. Johnson

cryogenic magnetometer shielded from the background magnetic field. Demagnetization protocol was determined using data from pilot samples and previous studies (Hicks et al., 2003; Clyde et al., 2016). Samples were first subjected to stepwise alternating field (AF) demagnetization via a Molspin tumbling AF demagnetizer at 3 milliTesla (mT) steps up to 30 mT; 5 mT steps between 30 and 60 mT; and, finally, 10 mT steps between 60 and 100 mT. AF demagnetization steps were applied until the natural remanent magnetization (NRM) fell below the detection level of the magnetometer or the NRM no longer decreased in intensity. Samples that did not have NRM completely removed according to AF protocol were then subjected to additional thermal demagnetization in an ASC Scientific Model TD-48SC thermal demagnetizer at the following temperature steps (in °C): 25, 80, 115, 135, 160, 250, 300, 350, 400, 450, 500, 525, 560, 580, 640, and 690.

Data Analyses

All sample data were analyzed using the PuffinPlot paleomagnetic data program (Lurcock and Wilson, 2012). Samples with three or more sequential steps exhibiting linear or quasi-linear decay to the origin were characterized using principle component analysis (PCA; Kirschvink, 1980). Only those samples with a maximum angular deviation of ≤ 20° were included (Figs. 2A–B). A Fisher mean (Fisher, 1953) was calculated for samples displaying an initial decay followed by strong clustering of vector endpoints and no further decay (Figs. 2C–D this paper). Some samples with overlapping unblocking spectra display a demagnetization path best characterized by a great circle (Fig. 2E). Additionally, some samples exhibited chaotic demagnetization behaviors and were not able to be characterized by the previously described methods (Fig. 2F). Site means characterized by three or more great circles or some combination of principle component analysis (PCA) and great circles were determined according to the analysis described in McFadden and McElhinny (1988) using the PuffinPlot program (Lurcock and Wilson, 2012).

Alpha sites for this study (Figs. 3A–C; Table S2) are described using Fisher statistics and defined as sites that pass the Watson test for randomness with the requisite *R*-value (Watson, 1956) and included three or more samples whose characteristic remanent magnetization (ChRM) was defined by either principle component or Fisher mean (or some combination). Beta sites are sites that have three or more sample directions, but include at least one sample characterized by great circle analysis (McFadden and McElhinny, 1988). Well characterized sample directions from sites that do not meet the alpha or beta criteria are still reported (Table S3) and considered in the magnetostratigraphic analyses.

Isothermal Remanent Magnetization

Seven samples from sites spanning the field area were selected to undergo isothermal remanent magnetization (IRM) experiments to better understand the mineralogy governing the magnetic remanence. To provide a comprehensive spread in lithologies and ages, samples were selected from sites within sections across the field area laterally as well as from one of the lower sections (Lyco-Luck) to the highest section stratigraphically (Kunstle). Additionally, this helped to test whether poorly behaved samples in the stratigraphically lower Lyco-Luck section differed significantly in magnetic mineralogy relative to well-behaved sites that are stratigraphically higher. The IRM samples were first cut into cubes < 1 cm^3. Then, the x-axis of each cube was subjected to a magnetic field of increasing strength within an ASC Scientific IM-10 impulse magnet at discreet steps from zero up to 1.1 Tesla (T) and measured in the 2G magnetometer after each step (Table S4). Upon reaching the 1.1 T step, the samples were then subjected to a backfield applied in the opposite direction in steps of 100 and 300 mT. This was done to isolate the proportion of remanence held by the soft and hard components. From the backfield magnetization, it is possible to determine the contributions to bulk remanence of hard antiferromagnetic components (e.g., hematite, goethite, etc.) and soft ferrimagnetic components (e.g., magnetite, maghemite, etc.) through the calculation of the S-ratio (Stober and Thompson, 1979; Bloemendal et al., 1992; Maxbauer et al., 2016). The S-ratio is defined as half of the difference between the saturation isothermal remanent magnetization (SIRM) and the IRM at 300 mT (IRM$_{-300mT}$), divided by the SIRM (Maxbauer et al., 2016). Following the three-axis IRM method of Lowrie (1990), a field of 1.1 T was then applied to the x-axis, 0.4 T to the y-axis, and 0.12 T to the z-axis of the samples to separate the magnetization of mineral fractions of different coercivities along each axis. The samples were then subjected to thermal demagnetization at the following temperature steps (°C): 25, 50, 86, 109, 132, 150, 209, 250, 275, 300, 325, 350, 375, 400, 500, 540, 560, 580, 600, 621, 650, and 680 (Table S5). The magnetic intensities of the three orthogonal axes were measured at each step and compiled into three-axis IRM demagnetization curves.

U–Pb Zircon Geochronology

Two Leaf 6 stratigraphic samples of volcanic ash from separate sites at Corral Bluffs were collected and analyzed for U–Pb zircon geochronology. Sample KJ0958 (locally known as the "Feral Llama ash") was collected within the section at 1,900 m elevation. Sample KJ1702 (locally referred to as the "Stock Tank ash") was collected ~960 m to the W-SW of KJ0958 at 1,930 m elevation. Both ash deposits are expressed as thin (< 1–2 cm), gray, lensy tonsteins within 10–20 cm thick lignite deposits, similar to ashes previously dated from the central part of the basin (Clyde et al., 2016). The limited occurrence of outcrop between the two ash locations does not expose the proper stratigraphic level to allow

tracing the ashes directly, but sufficiently exposes adjacent horizons to show the gradual change of apparent dip from the Leaf 6 location (about 2° east) to the Stock Tank location (about 4–5° east). This simple change in apparent dip is consistent with a single ash layer having produced the measured elevation difference between the two age-dated locations. We interpret these ashes to represent the same volcanic deposit based on (1) the similar mode of occurrence of the two tephras; (2) the similar succession of coal-bearing and arkosic strata at the two ash locations; and (3) the structural dip model between the two locations (Supplement Figure S1 [Fig. S1]). This interpretation is reinforced by the observation that samples KJ0958 and KJ1702 have yielded ^{206}Pb /^{238}U ages that are equivalent within uncertainty (see Results section below).

Sample KJ0958 was processed and analyzed at the Massachusetts Institute of Technology Isotope Laboratory using the chemical abrasion-isotope dilution-thermal ionization mass spectrometry (CA-ID-TIMS) method. Sample KJ1702 was processed and analyzed at the Boise State University Isotope Geology Laboratory using tandem laser ablation-inductively coupled plasma-mass spectrometry (LA-ICP-MS). Detailed analytical methods for both samples can be found in the Supplement. U–Pb zircon age errors are reported for both samples in the form ± X/Y/Z where X is analytical error, Y is both analytical and tracer calibration error, and Z is the combined analytical, tracer, and decay constant uncertainty. The latter facilitates comparison of our reported ages with those derived from other decay schemes.

Palynological Analysis

Palynological analyses were conducted on a total of 46 samples from three sections to identify the placement of the K–Pg boundary in the study area: Bishop Wash (ADB1701 and ADB1702), Leaf 6 (ADB1703), and 9789 (ADB1802). Samples were processed by Global Geolab Limited, Medicine Hat, Canada, using standard palynological procedure. Approximately 20 gm of bulk rock was treated with dilute hydrochloric acid (HCl), macerated in 75% hydrofluoric acid, and cleaned of fluorosilicate byproducts in hot HCl. Organic residue was sieved, the fraction between 10 µm and 200µm was kept, dyed with safranin red, and mounted in polyester resin on one or two microscope slides, depending on recovery.

Slides are reposited at the Denver Museum of Nature & Science (DMNS). Organic matter recovery ranges from excellent to fair, with some barren samples and some samples showing a significant amount of older reworked palynomorphs. The position of the K–Pg boundary is determined both by the last occurrence (LAD) of typical Cretaceous taxa (K-taxa) and by the first occurrence (FAD) of typical Paleocene taxa (Nichols et al., 2002). Bercovici et al. (2009) observed that K-taxa often cross the boundary in low num-

bers, even at K–Pg sections that preserve the physical evidences of the Chicxulub impact (boundary clay and spherules) such as Mud Buttes in southwestern North Dakota. The persistence of few K-taxa above the boundary can be accounted as small-scale reworking or as short-term persistence, as such the use of presence and absence data alone can lead to a stratigraphic over-estimation of the placement of the K–Pg boundary. Bercovici et al. (2009) proposed to use relative abundance counts, where the K–Pg is identified by a major decrease of the relative abundance of K-taxa without subsequent recovery, from ~10–30% as typical values in Cretaceous samples, to < 1% in the Paleocene. Stratigraphic reworking of Cretaceous sediments and K-taxa up-section is a high possibility at Corral Bluffs since many samples also show reworked marine dinoflagellates from the Pierre Shale, and also Permian palynomorphs. Moreover, Paleocene indicator taxa that appear after the K–Pg are less likely to be reworked down-section. Paleocene samples are characterized by the appearance of several pollen species belonging to the *Momipites* genus. The K–Pg boundary is placed midpoint between the highest-Cretaceous sample and the lowest-Paleocene sample.

RESULTS

Paleomagnetism

Demagnetization Behavior

The majority of samples responded favorably to the AF demagnetization protocol, with only one site (CB1703B) needing additional thermal steps to be fully characterized. Thermal demagnetization applied after AF demagnetization did not prove to be effective for the vast majority of samples as the remaining high-coercivity component typically did not exhibit clear demagnetization behavior when subjected to these additional thermal steps. This was likely due to the presence of goethite, which was observed in some IRM samples (see below). Of the 426 samples that were analyzed, 185 displayed a linear decay to the origin with characteristic ChRMs defined by PCAs with maximum angular deviations ≤ 20° (Figs. 2A–B). One-hundred and twenty-one samples exhibited initial decay followed by strong clustering of vector endpoints that were calculated using Fisher means (Figs. 2C–D). Sixty-nine samples were characterized by great circle analysis due to the overlapping unblocking spectra between the components of the NRM of samples (Fig. 2E). The 51 remaining samples were not able to be characterized due to highly chaotic demagnetization behavior (Fig. 2F).

Site Calculations

Of the 134 sites for which three or more samples were analyzed, 84 fit the criteria for alpha sites, whereas 23 are considered beta (Table S2). Some sites did not meet the alpha
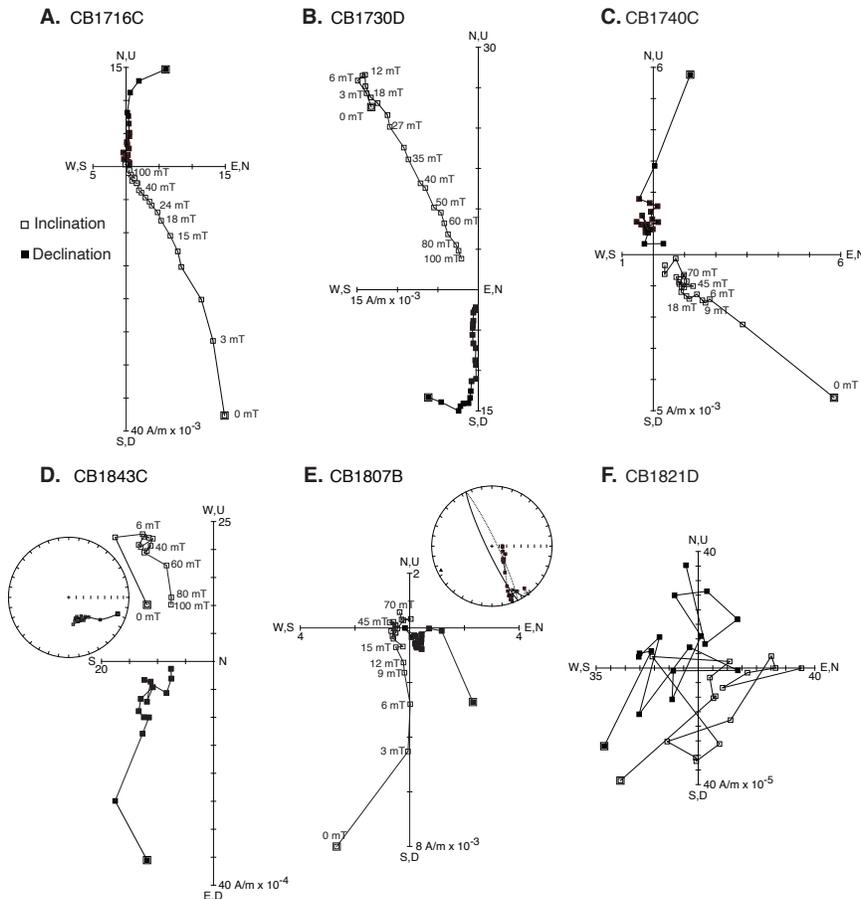
Anthony J. Fuentes, William C. Clyde, Ken Weissenburger, Antoine Bercovici, Tyler R. Lyson, Ian M. Miller, Jahandar Ramezani, Vincent Isakson, Mark D. Schmitz, and Kirk R. Johnson

Figure 2. Representative vector endpoint diagrams for selected samples. Vector endpoints are labeled with alternating field intensity in milliTesla (mT). **A–B,** CB1716C (normal polarity sample) and CB1730D (reversed polarity) show linear decay toward the origin and are characterized by PCA. **C–D,** CB1740C (normal polarity) and CB1843C (reversed polarity) exhibit clustering of vector endpoints and are characterized by a Fisher mean (Fisher, 1953). Adjacent equal area projection for CB1843C, illustrating clustering of vector endpoints. **E,** CB1807B is a reversed polarity sample exhibiting a direction best characterized by the great circle analysis of McFadden and McElhinny (1998). Equal area projection for CB1807B with a great circle defining sample ChRM is inset adjacent to that sample's vector endpoint diagram. **F,** CB1821D is a sample exhibiting chaotic demagnetization behavior and was not able to be characterized using a PCA, Fisher mean, or great circle analysis.

or beta criteria, but they still contained samples with stable demagnetization. These sample ChRM directions are plotted in their respective sections' magnetostratigraphic plots to help further guide our interpretation. Polarity determinations were not possible for sites CB1818, 1819, 1822, 1849, 1852, 1862, 1874, and 1876 due to highly chaotic behaviors of the samples; thus, these were not considered further for analyses.

Reversal Test

The reversal test is a standard field stability test in paleomagnetism that determines whether the two polarities in a paleomagnetic data set are antipodal to one another as one would expect under the geocentric axial dipole model of the Earth's magnetic field (Cox and Doell, 1960; Heslop

and Roberts, 2018). The mean declination and inclination of the normal polarity alpha sites is 351.9/58.4, and the overall mean for all normal polarity alpha and beta sites is 349.1/57.8. The mean declination and inclination for the reversed polarity alpha sites is 162.7/-46.9, and the mean for all reversed polarity sites is 164.4/-48.3. The 83 alpha sites of both normal and reversed polarities narrowly passed the parametric bootstrap reversal test of Tauxe et al. (2018) at the 95% confidence level as signified by the slight overlap of the α95s of the two populations of directions (Figs. 4A–B). The narrow passage of the reversal test is likely due to a small—but persistent—present-day normal polarity overprint causing reversed polarity samples to have slightly shallower inclinations than normal polarity samples and potentially steeper than expected inclinations for normal polarity samples.
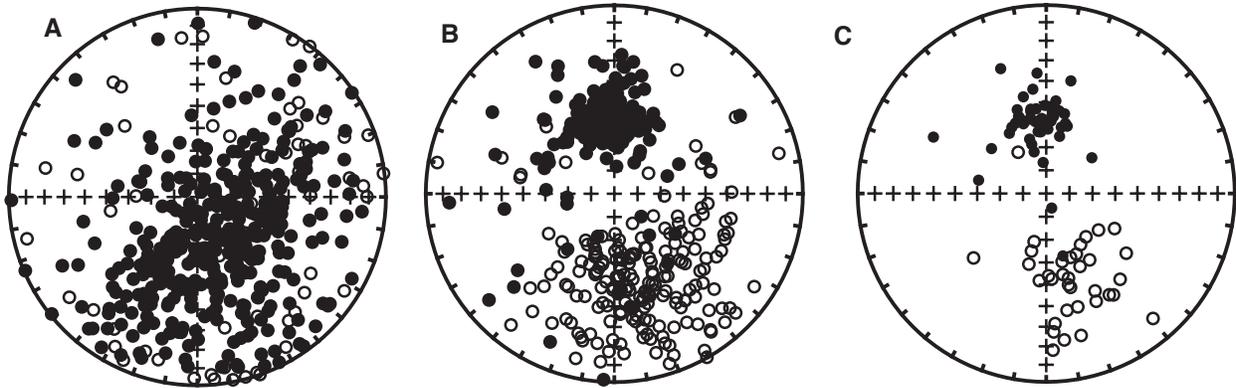
Figure 3. Equal area projections for paleomagnetic sample and alpha site directions. **A,** Equal area projections of all NRM paleomagnetic sample directions. **B,** ChRM directions for paleomagnetic samples with coherent demagnetization behavior. **C,** Alpha site mean ChRM directions.
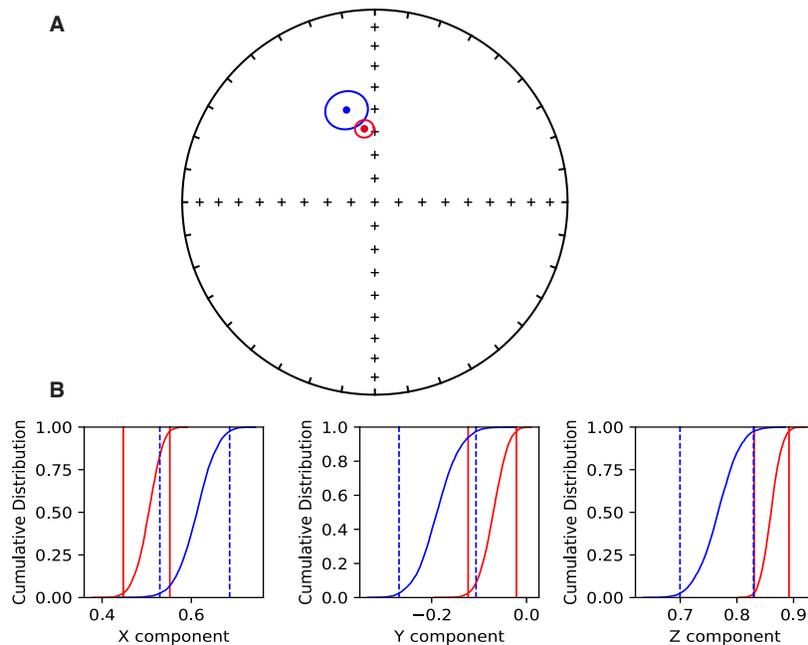

Figure 4. A, Mean ChRM directions of alpha normal polarity sites (red) and alpha reversed sites flipped to antipodal direction (blue) with overlapping α95 confidence ellipses. **B,** Results of the parametric bootstrap reversal test of Tauxe et al. (2018) showing the overlap of X, Y, and Z components in Cartesian coordinates. Solid red and dashed blue lines correspond to the α95 confidence interval for normal and reversed sites, respectively.

Polarity Determinations and Reversal Placement

Polarity determinations for most sites are very clear so paleomagnetic reversals are positioned stratigraphically halfway between two superpositionally adjacent alpha or beta sites of opposite polarity (Table S2). The 9776 section exhibits a polarity oscillation close to a reversed-to-normal polarity reversal near the base of the section (Table S2). Sampling of this interval was undertaken along a short ridge, where no slumping was apparent. It is likely that the oscillation in polarity corresponds to an instability in the geomagnetic field near the paleomagnetic reversal or a persistent overprint modern normal polarity overprint. In this case, the paleomagnetic reversal was placed above the highest reversed site and below the subsequent normal site.

Nine of the 10 sections recorded at least one polarity reversal. The lowest sections (Lyco-Luck, Leaf 6, and lower portion of 9789) exhibit a normal polarity interval that switches to reversed polarity at an average elevation of 1,887 m. Most of the stratigraphically higher sections (Bambino Canyon, 9776, upper portion of 9789, JZ composite, Bishop

Wash, and Waste Management) record a reversed polarity interval at the base of the sections that switches to a normal polarity interval at an average elevation of 1,952 m. The Hawkins section is entirely characterized by reversed polarity. The highest section stratigraphically (Kunstle) has a normal polarity zone at the base that transitions to reversed polarity at ~2,039 m elevation. The 9789 section includes two paleomagnetic reversals, from normal to reversed polarity at ~1,880 m elevation and from reversed to normal at 1,960 m (Table S2).

Paleomagnetic Pole

The paleomagnetic pole calculated from the alpha sites (with reversed polarity sites inverted) is 135.3°/81.3° (α95 = 4.7°) and does not overlap with the unflattened or flattened paleomagnetic poles of North America from 70 to 60 Ma (Besse and Courtillot, 2003; Torsvik et al., 2012). Several factors may be causing this discrepancy. Inclination shallowing and a weak, but persistent, present-day overprint causing shallower than expected directions for reversed sites are likely the predominate contributors to the somewhat "far-sided" pole for this study. The paleomagnetic pole from Sprain et al. (2018) in the Hell Creek area of Montana overlaps with the α95 of our paleomagnetic pole (Fig. 5) and is similarly far-sided relative to the North American poles during this interval (Besse and Courtillot, 2003; Torsvik et al., 2012).

Isothermal Remanent Magnetization Experiments

The IRM acquisition curves for all samples from Corral Bluffs are characterized by a steep increase in intensity up to ~300 mT, which is consistent with low-coercivity species such as magnetite, titanomagnetite, and maghemite (Figs. 6A–B; Figs. S2A–G). The S-ratios calculated from the backfield steps (Maxbauer et al., 2016) are all > 0.5, which is also indicative of a majority of the bulk remanence held by low-coercivity components (Fig. 6C). CB1824B, CB1827B, and CB1869B show small increases in intensity past 300 mT, which is indicative of the presence of higher coercivity minerals such as hematite and goethite (Figs. S2E–G). The backfield data for these samples show that, although these samples are influenced by a high-coercivity component, they all have S-ratios > 0.8 so are still dominated by a low-coercivity phase.

The three-axis IRM demagnetization curves indicate that the soft axis (0.12 T) in all samples initially have by far the highest intensity, which is consistent with remanence held by low-coercivity minerals (Figs. S2A–G). There is a considerable drop in intensity along the 0.12 T axis of all the samples from 200–500°C followed by generally another significant drop from 540–580°C, at which point the intensity of the soft axis of the samples is essentially null. It is difficult to distinguish between the acquisition and demagnetization properties of magnetite and either titanomagnetite or titanomaghemite. The latter two have coercivities that are approximate to that of magnetite and can have unblocking
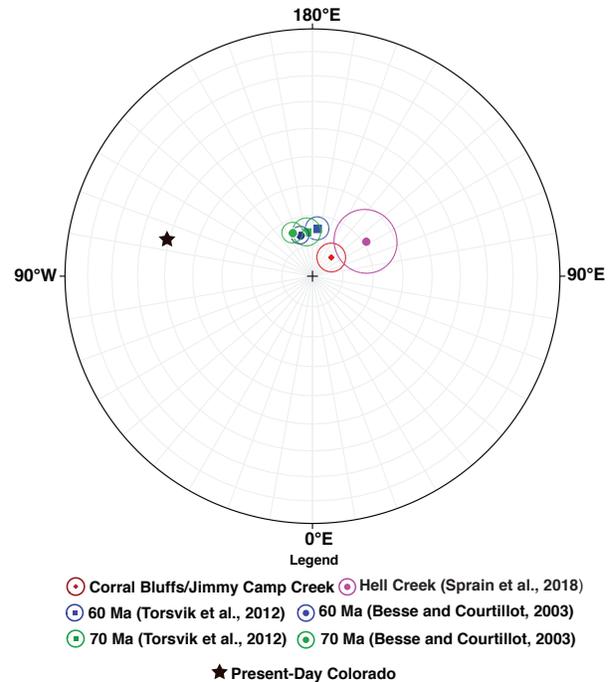

Figure 5. Polar equal area projection showing the paleomagnetic pole for this study (red diamond) plotted with its α95 confidence interval. 70 Ma (green) and 60 Ma (blue) paleomagnetic poles with corresponding α95 confidence intervals for Laurentia (North America and Greenland) from Besse and Courtillot (2003) (circles) and Torsvik et al. (2012) (squares). Magenta circle represents the paleomagnetic pole of Sprain et al. (2018). Black star represents the location of present-day Colorado relative to the poles.

temperatures ranging from room temperature to > 600°C (Özdemir and Banerjee, 1984; Lowrie, 1990). Given the fluvial depositional environment of the sediment at the field site, it is likely that the primary low-coercivity component is detrital magnetite/titanomagnetite eroded and deposited during the uplift of the Front Range. Maghemite is also likely present in these rocks as it often forms as a product of oxidation of magnetite, either through weathering or pedogenic processes (van Velzen and Dekkers, 1999). Additionally, Sprain et al. (2016) noted the presence of intermediate titanohematite, a secondary carrier of remanence in sediments spanning the K–Pg boundary in the Hell Creek area of Montana and demonstrated that intermediate titanohematite is more common than initially suspected in Laramide-aged deposits. The three-axis demagnetization curves of the sediments from Corral Bluffs are similar to those in Sprain et al. (2016), indicating the likeliness of some intermediate titanohematite component within the sediments from Corral Bluffs, but the dominant carrier of primary remanence is detrital titanomagnetite. CB1821D, CB1824B, and CB1869B show a slight dip in intensity along the hard axis (1.1 T) between 50–150°C, which is evidence
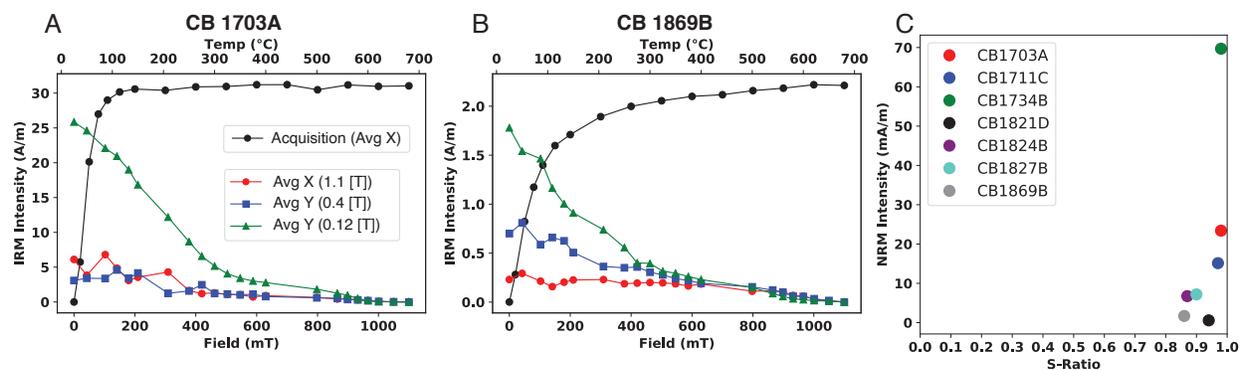
Figure 6. IRM acquisition (black line, bottom axis) and three-axis thermal demagnetization curves (colored lines, top axis) for two representative samples. **A,** CB1703A showing sample dominated by magnetite. **B,** CB1869B showing sample dominated by magnetite, but influenced by minor amounts of hematite. **C,** NRM intensity (mA/m) vs S-ratio for all IRM samples showing that remanence in all samples was carried dominantly by a low coercivity mineral interpreted to be magnetite. See Supplement Figure S2 (Fig. S2) and Tables S4–S5 for complete IRM data.

of a small amount of goethite within these samples (Figs. S2D–E, G). CB1824B, CB1827B, and CB1869B have the smallest S-ratios (Fig. 6C). These three samples, including CB1869B (Fig. 6B), show a final decrease in intensity along the hard axis above the 580°C step (Figs. S2E–G). This is characteristic of hematite, which is the primary hard coercivity component within these samples. The minor amounts of goethite and hematite in these samples indicate that these facies likely underwent weak pedogenesis soon after deposition. The weak, but persistent, modern overprint is likely held by some combination of goethite, hematite, and potentially intermediate titanohematite as this secondary component is not completely removed via AF demagnetization. This high-coercivity secondary overprint exhibited poor demagnetization behavior when subjected to additional thermal stepwise demagnetization, which is supportive of goethite as a primary carrier of secondary remanence.

U–Pb Zircon Geochronology

Sample KJ0958 ('Feral Llama' ash)

All seven zircon crystals selected and analyzed by CA-ID-TIMS from the Corral Bluffs ash bed define a statistically coherent cluster of $^{206}Pb/^{238}U$ dates with a weighted mean date of 66.253 ± 0.031/0.045/0.084 Ma and a mean squared weighted deviation (MSWD) of 0.36. This date best represents the age of zircon crystallization and a good approximation for the age of sample KJ0958, Feral Llama ash deposition (Fig. 7A; Table S6).

Sample KJ1702 ('Stock Tank' ash)

Most of the zircon population of sample KJ1702 (Stock Tank ash) consists of large (majority greater than ~100 μm), generally euhedral grains, many of which possess dark inherited cores in cathodoluminescence imagery. Thirty-five LA-ICP-MS analyses yielded $^{206}Pb/^{238}U$ dates from 77 to

61 Ma, and the aforementioned cores yielded Precambrian dates > 1400 Ma (Table S7).

Ten zircon grains lacking obvious inherited cores were selected from the youngest LA-ICP-MS population and successfully analyzed by CA-ID-TIMS. Two grains (z5 and z11) yielded older, concordant dates of ~66.5 Ma and are attributed to subtly older magmatism. The remaining eight CA-ID-TIMS analyses provide a weighted mean $^{206}Pb/^{238}U$ date of 66.252 ± 0.018/0.038/0.081 Ma (MSWD = 0.49). This is interpreted to represent the age of zircon crystallization and a robust estimate of the eruption and deposition of the ash sample (Fig. 7A; Table S8).

Palynology

Palynological assemblages from the lower portions of the Leaf 6, 9789, and Bishop Wash sections correspond to the upper Maastrichtian *Wodehouseia spinata* Assemblage Zone (Nichols, 1994; Bercovici et al., 2012). The sharp decline in relative abundance without subsequent recovery (Bercovici et al., 2009) of typical Cretaceous taxa, or K-taxa (Nichols et al., 2002), is indicative of the terrestrial floral demise associated with the K–Pg boundary and the Chicxulub impact (Nichols and Johnson, 2002, 2008; Vajda and Bercovici, 2014; Fastovsky and Bercovici, 2016). The identified K-taxa from Corral Bluffs are *Aquilapollenites calvus*, *A. turbidus*, *A. collaris*, *A. conatus*, *A. marmarthensis*, *A. mtshedlishvili*, *A. quadrilobus*, *A. reductus*, *A. trialatus, Ephedripites multipartitus*, *Erdtmanipollis* spp., *Libopollis jarzeni*, *Liliacidites altimurus*, *Liliacidites complexus*, *Retibrevitricolporites beccus*, *Striatellipollis striatellus*, *Tricolpites microreticulatus*, and *Tschudypollis* spp. In addition to the above pollen taxa, the epiphyllous fungal thallus *Trichopeltinites* sp. is also present, and sometimes very common with relative abundance of up to 59.8%. *Trichopeltinites* has been reported to disappear at the K–Pg boundary, presumably along with its macrofloral host (Nichols and Johnson, 2008);
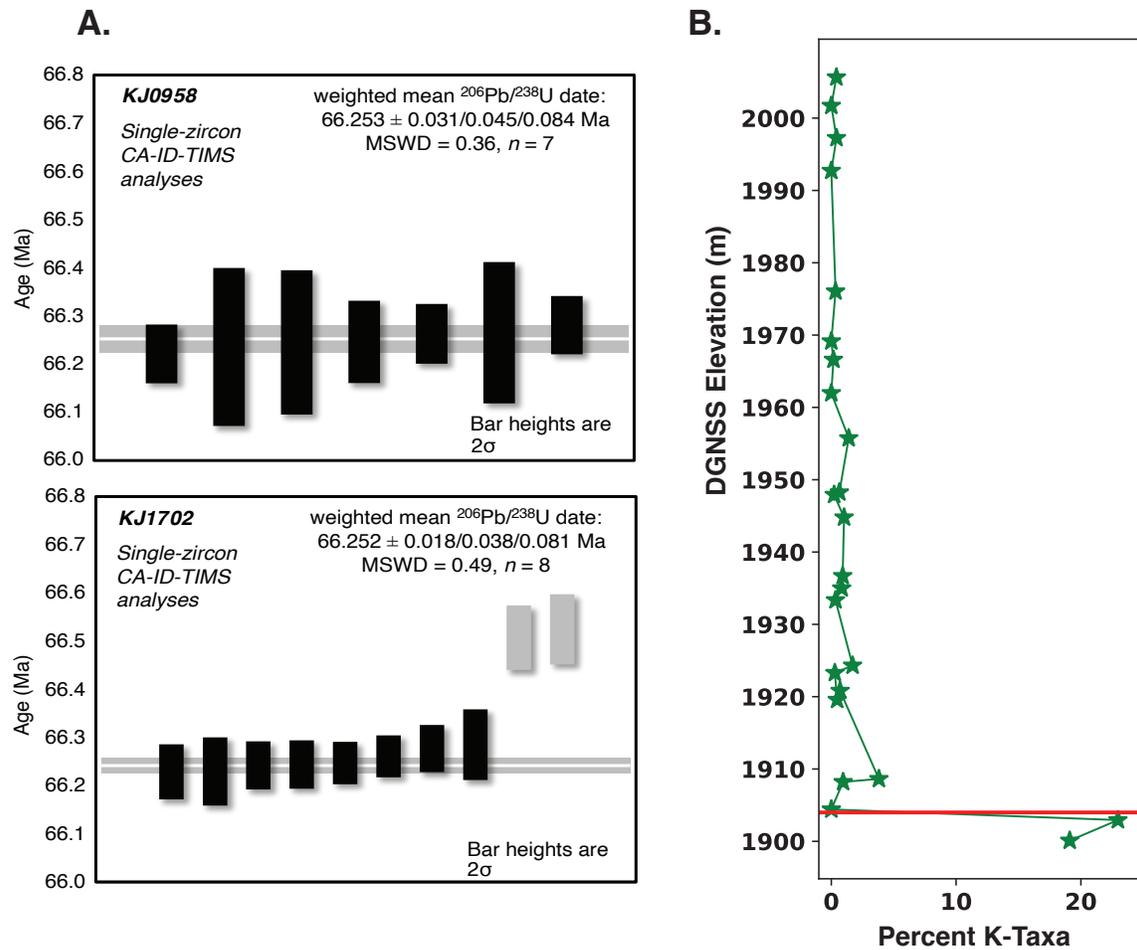
Anthony J. Fuentes, William C. Clyde, Ken Weissenburger, Antoine Bercovici, Tyler R. Lyson, Ian M. Miller, Jahandar Ramezani, Vincent Isakson, Mark D. Schmitz, and Kirk R. Johnson

Figure 7. Palynological and ^{206}Pb /^{238}U age constraints. **A,** Distribution of ^{206}Pb/^{238}U ages of analyzed zircons from the Feral Llama (KJ0958) and Stock Tank (KJ1702) ash beds at Corral Bluffs . Vertical bars represent individual zircon analyses with the bar height proportional to 2σ analytical uncertainty of the ^{206}Pb/^{238}U dates. Solid bars are analyses used in date calculation. Horizontal line and its shaded envelope signify the weighted mean date and its 95% confidence level uncertainty, respectively. See Tables S6 and S7 for complete U–Pb isotopic data and the Supplement for explanation of stated uncertainties. **B,** Percent of Cretaceous palynomorph counts per sample plotted by DGNSS elevation for the Bishop Wash section. Red line represents placement of K–Pg boundary in this section.

thus, it has been treated here as a K-taxon. The relative drop in abundance in K-taxa and the palynologically defined K–Pg boundary is clearly identified between samples ADB1701-0a and ADB1701-01 at Bishop Wash; ADB1703-04d and ADB1703-04e at Leaf 6; and ADB1802-06 and ADB1802-07 at 9789 (Figs. 7B, 8; Fig. S3; Table S9). Samples from above the boundary show the appearance of typical Paleocene *Momipites*, and low-diversity assemblages often dominated by palm pollen (*Arecipites* spp.).

DISCUSSION

Correlations of Paleomagnetic Reversals to GPTS

Biostratigraphic indicators from the Corral Bluffs field site such as fragmentary dinosaur remains, numerous Late Cretaceous and early Paleocene leaf localities (Johnson et al., 2003), and mammal fossils tentatively assigned to Pu2/Pu3 (Eberle, 2003), constrain the D1 strata in this part of the Denver Basin to the time interval from the latest-Cretaceous to the early Paleocene, as demonstrated by the basin-wide chronostratigraphy of Clyde et al. (2016). The integrated palynological and high-precision U–Pb geochronological results reported here and tied to specific stratigraphic sections provide further support for this interpretation. The results of the integrated analyses presented here constrain the correlation of the magnetostratigraphic data to the geomagnetic polarity time scale (GPTS) and identify a precise position of the K–Pg boundary across the field area.

East of Jimmy Camp Creek, at Corral Bluffs, are the Bishop Wash, Leaf 6, and 9789 sections (Fig. 1B), where the three palynologically determined K–Pg boundary sites from

this study are located at approximately 1,904, 1,925, and 1,910 m elevation, respectively (Figs. 7B, 8; Fig. S3; Table S9). Fragmentary ceratopsian dinosaur material (DMNH Loc. 4195) was also identified at 1,924 m in the Leaf 6 section. A ^{206}Pb /^{238}U age of 66.253 ± 0.031/0.045/0.084 Ma was obtained from zircon grains within the Feral Llama ash (KJ0958) at an elevation of 1,900 m within the Leaf 6 section (Figs. 1B, 7A; Fig. S1). An identical (within uncertainty) ^{206}Pb /^{238}U age of 66.252 ± 0.018/0.038/0.081 Ma was independently obtained for sample KJ1702 from the Stock Tank ash at a site ~1 km to the west in an area where no paleomagnetic data were collected (Figs. 1B, 7A; Fig. S1). KJ1702 provides temporal constraints to nearby fossil localities in this area and supports our stratigraphic model indicating that the two ashes are actually from the same volcanic deposit, which allows for these localities to be directly correlated to the Leaf 6 section (Figs. 1A–B; Fig. S1).

Hicks et al. (2003) previously identified paleomagnetic reversals corresponding to the interval from C31n and C30n–C29r in their Jimmy Camp Creek section, the top of which overlaps with our Lyco-Luck section. The normal polarity zone within the Lyco-Luck section is interpreted to correspond to the upper portion of C30n with a subsequent reversed interval interpreted as C29r (Fig. 8). Further up-section in Jimmy Camp Creek, the Bambino Canyon and 9776 sections record basal reversed intervals followed by normal polarity intervals (Fig. 8). Due to their clear positions stratigraphically higher than the Lyco-Luck section, the reversed polarity intervals are interpreted to correlate to C29r and the normal polarities to C29n (Fig. 8).

At the base of the Leaf 6 and 9789 sections are normal polarity zones corresponding to C30n on the basis of their position below reversed intervals containing the K–Pg boundary correlating to C29r on the GPTS (Fig. 8). The 9789 section records a second polarity reversal from reversed polarity to normal polarity near the top of the section and is correlated to the C29r–C29n reversal based on its position above the C30n–C29r reversal. The high density of sampling through the C29r interval exhibiting uniform polarity until the overlying C29r–C29n reversal further supports this interpretation. (Fig. 8).

Continuing eastward, the JZ composite section—comprising the JZB and Hilaire-West subsections (Figs. 1B, 8; Table S2)—overlaps with the 'JZ section' of Hicks et al. (2003). We sampled within the gap between the highest reversed polarity site and lowest normal polarity site in the JZ section of Hicks to increase the resolution in this section. We also sampled higher via the Hilaire-West subsection. Our data agree with the determination of Hicks et al. (2003) that the transition from the reversed polarity zone to the normal polarity zone represents the C29r–C29n boundary based upon stratigraphic relationships (Fig. 8). The gap in our sampling was previously shown to represent C29n by Hicks et al. (2003) and was not resampled as the

C29n–C28r reversal was clearly higher than their JZ section.

The stratigraphically highest section in our field area is Kunstle, east of the Hilaire-West subsection. This section records a normal polarity interval through the base of the section, followed by a reversed polarity interval and ending with mixed polarity at the very top (Fig. 8). Traverses on marker beds stratigraphically tie the Kunstle section to the adjacent Hilaire-West subsection. This indicates that the normal interval at the base of Kunstle corresponds to C29n, and the overlying reversed polarity zone correlates to C28r. Site CB1854 is a normal polarity site located above three reversed polarity sites and below another reversed polarity site, indicating that this site may either have a strong normal overprint or may have captured a short interval of instability in the Earth's magnetic field at this time, possibly related to the next reversal. No slumping was apparent across the ridge where CB1854 was sampled, and the sites are clearly in superposition.

The Bishop Wash section records the third palynologically determined K–Pg boundary near the base of the section at an elevation of ~1,904 m, within a reversed polarity interval assigned to C29r (Fig. 8). The high resolution of sampling through this section indicates that the subsequent normal polarity zone must represent C29n.

The Waste Management section records a paleomagnetic reversal from reversed to normal polarity. It is interpreted that this reversal represents the C29r–C29n boundary given the stratigraphic position of the section relative to the Bishop Wash section (Fig. 8). The easternmost section, Hawkins, is directly across Colorado State Highway 94 from the Waste Management section (Fig. 1B) and is characterized by a reversed polarity zone throughout the entire section. The Hawkins section is stratigraphically below the adjacent Waste Management section where we identified the C29r–C29n reversal; therefore, the reversed zone making up the entirety of this section is interpreted to be the C29r subchron (Fig. 8).

The patterns of reversals observed at Corral Bluffs and Jimmy Camp Creek are correlated here to the interval C30n–C28r, with both the top and bottom of C29r observed within the 9789 section. The chron boundaries occur at very similar elevations across the entire field area, which agrees well with the nearly flat-lying beds observed in the field (Fig. 8). The proportional thicknesses of the chron boundaries and the K–Pg boundary matches well with the GPTS of Gradstein et al. (2012), which is supportive of the Corral Bluffs area preserving a near continuous depositional sequence that is not disrupted by significant unconformities.

Correlations to Basin-Wide Magnetostratigraphic Framework

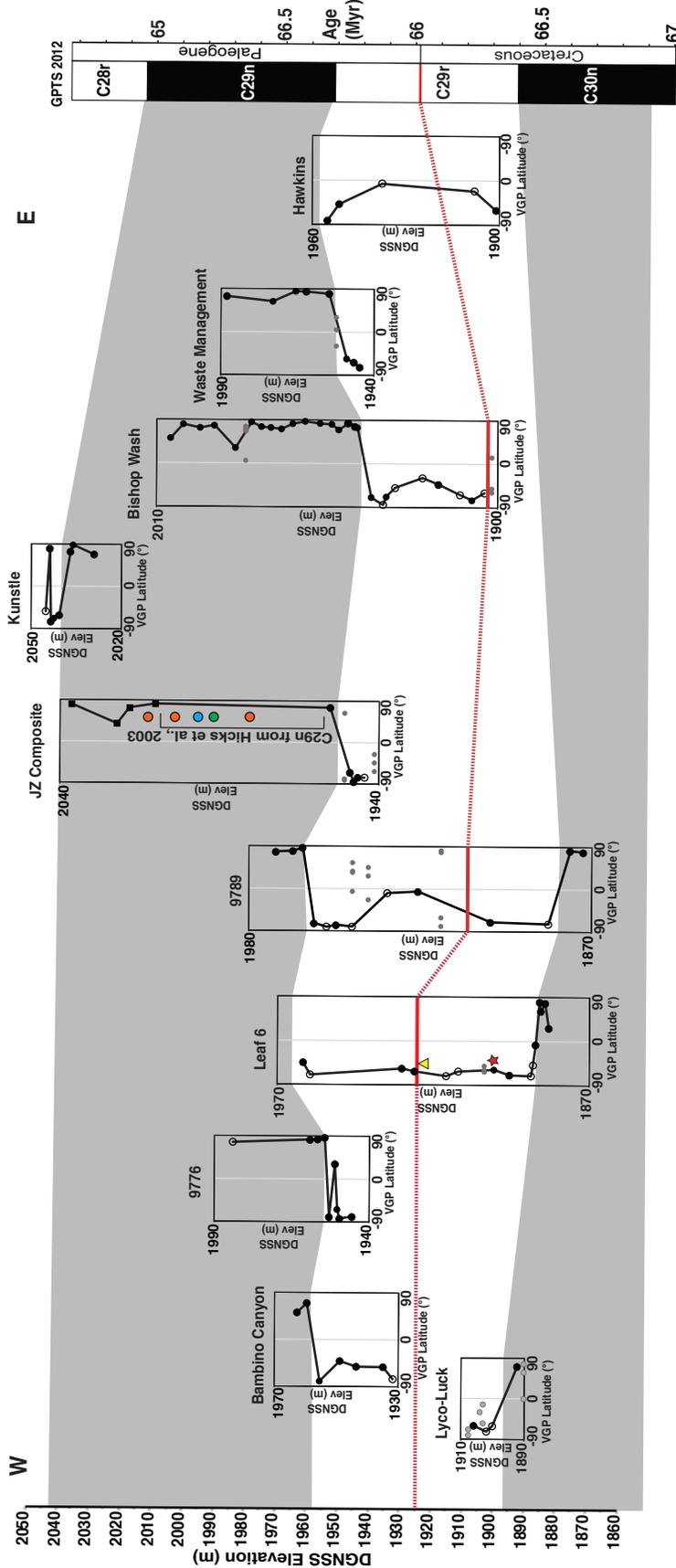The pattern of paleomagnetic reversals identified at Corral Bluffs and Jimmy Camp Creek from this study and

Anthony J. Fuentes, William C. Clyde, Ken Weissenburger, Antoine Bercovici, Tyler R. Lyson, Ian M. Miller, Jahandar Ramezani, Vincent Isakson, Mark D. Schmitz, and Kirk R. Johnson

Figure 8. West-to-east fence diagram of Corral Bluffs with magnetostratigraphic sections plotted by elevation and correlated to the geomagnetic polarity time scale of Gradstein, 2012. Paleomagnetic section names labeled above respective virtual geomagnetic pole (VGP) plots. Shaded regions correspond to the normal polarity chrons 30n and 29n. Closed circles are alpha-level sites, and open circles are beta-level sites. Small, gray circles are samples with stable demagnetization that are from sites that did not pass the Watson test. Solid red line is the K–Pg boundary where determined through palynological analysis. Dashed red line represents inferred level of K–Pg across the field area. Bracketed zone in the JZ composite section was previously identified as C29n by Hicks et al. (2003). Red star represents location of ^{206}Pb/^{238}U dated Feral Llama ash (KJ0958; 66.253 ± 0.031/0.045/0.084 Ma). Yellow triangle is the location of the fragmentary ceratopsian dinosaur remains within Leaf 6 (DMNH [Denver Museum of Nature & Science] loc. 4195). Circles mark the approximate locations of the Pu2/Pu3 mammal localities (orange - DMNH loc. 2555, 2544, and 2554), a vertebrate microsite (green - DMNH loc. 2551= UCM [University of Colorado Museum of Natural History] loc. 77278), and a crocodilian skull (blue - DMNH loc. 2548) described in Eberle, 2003.
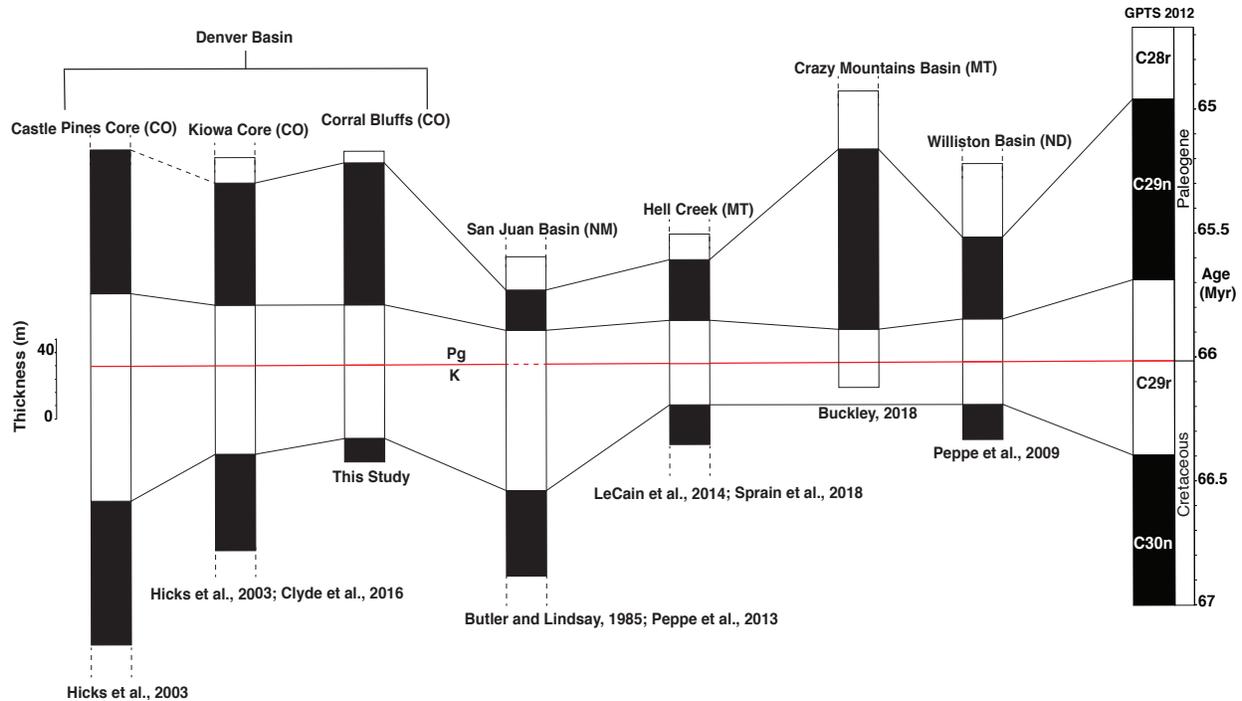
Figure 9. Magnetostratigraphic correlations of the K–Pg boundary interval (top of chron C30n–C28r) from the Castle Pines core (Hicks, et al., 2013), Kiowa core (Hicks et al., 2003; Clyde et al., 2016), and Corral Bluffs (this study) to studies in the San Juan Basin (Butler and Lindsay, 1985; Peppe et al., 2013), Hell Creek region of Montana (LeCain et al., 2014; Sprain et al., 2018), Crazy Mountains Basin of Montana (Buckley, 2018), and Williston Basin in North Dakota (Peppe et al., 2009). Solid red line represents the K–Pg boundary as defined in the respective studies. K–Pg boundary dashed line in San Juan Basin magnetostratigraphy represents uncertainty in the placement of boundary (Peppe et al., 2013). Dashed vertical lines indicate that sections continue further in those studies than is shown here. Dashed line from Castle Pines core to Kiowa core indicates that the C29n–C28r boundary is not preserved in the Castle Pines core; therefore, the top of C29n is approximated. Solid black lines represent correlations of the paleomagnetic reversal boundaries across the studies to the GPTS of Gradstein et al., 2012. All sections plotted to same stratigraphic scale with approximate thickness scale shown (m).

Hicks et al. (2003) is interpreted to represent the interval from chrons C31n and C30n–C28r. This represents the longest surface exposure in the Denver Basin for which there are chronostratigraphic constraints. The Kiowa core matches closely with these results as it likewise records C31n and C30n–C28r (Hicks et al., 2003; Clyde et al., 2016). The short reversed polarity interval C28r is not recorded in the thicker Castle Pines core, where it is thought to be cut out by a thick channel sandstone (Hicks et al., 2003). It is also possible to correlate the three surface sections of Clyde et al. (2016) from the central part of the basin to our sites as these sections span the interval from C29r to C28n (Fig. 9).

Paleontological Implications

Given the reported provinciality of mammalian faunas during the Puercan (Lofgren et al., 2004), it is critical to the understanding of regional recovery dynamics to have independent age controls at key fossil localities to correlate coeval faunas across the Western Interior. It is now possible to tie our new magnetostratigraphy at Corral Bluffs to other key K–Pg boundary sites in the Western Interior (Butler and Lindsay, 1985; Swisher et al., 1993; Peppe et al., 2009; LeCain et al., 2014; Sprain et al., 2018; Buckley, 2018; our Fig. 9).

The Pu1 localities identified in the Denver Basin occur within C29r. This includes the Alexander locality, which is thought to represent an intermediate between Pu1 and Pu2 faunas (Eberle, 2003; Hicks et al., 2003; Middleton and Dewar, 2004; Dahlberg et al., 2016). The Hell Creek region in Montana's Garfield and McCone counties has yielded Pu1 and Pu3 mammal fossils and is among the best paleontologically sampled K–Pg boundary intervals with extensive chronostratigraphic controls (Swisher et al., 1993; Clemens, 2013; LeCain et al., 2014; Wilson, 2014; Sprain et al., 2015, 2018). Swisher et al. (1993) and LeCain et al. (2014) identified paleomagnetic reversals interpreted to represent C30r–C28n within the Hell Creek and Fort Union Formations in Garfield and McCone counties. Sprain et al. (2018) further refined the magnetostratigraphy of the Hell Creek region across 14 sections that are interpreted to span C30n through C29n. Pu1 assemblages within the Hell Creek region of

Anthony J. Fuentes, William C. Clyde, Ken Weissenburger, Antoine Bercovici, Tyler R. Lyson, Ian M. Miller, Jahandar Ramezani, Vincent Isakson, Mark D. Schmitz, and Kirk R. Johnson

Montana are located within C29r. The Hanna Basin in Wyoming, which is the only locality that preserves Lancian through Pu3 localities in direct superposition, does not as of yet have a magnetostratigraphy in which to place these localities (Lillegraven and Eberle, 1999).

The Pu2/Pu3 fauna of Corral Bluffs described by Eberle (2003) and Middleton (1983) were sampled from the C29n interval of Hicks et al. (2003), which correspond to our JZ composite section. Our new magnetostratigraphic results support this determination (Fig. 8). The Nacimiento Formation in the San Juan Basin of New Mexico is the type locality for the Puercan and is currently known to possess assemblages interpreted to correspond to Pu2 and Pu3 located within a normal polarity zone also interpreted as C29n (Butler and Lindsay, 1985; Williamson, 1996; Lofgren et al., 2004; Peppe et al., 2013). The Pu3 localities from the Hell Creek area are also interpreted to lie within C29n (Sprain et al., 2018). Magnetostratigraphic results from the eastern Williston Basin in North Dakota complicate the associations observed elsewhere (Hunter and Archibald, 2002; Peppe et al., 2009). The Pu2 fauna from the Williston Basin's PITA Flats locality is interpreted to occur within C29r based upon its proximity to the K–Pg boundary (Hunter and Archibald, 2002; Fox and Scott, 2011). The Pu2 Hiatt local fauna from Makoshika State Park in eastern Montana is located within C29r (Hunter et al., 1997). Pu2 assemblages from the Rav W-1 horizon of the Ravenscrag Formation in southwestern Saskatchewan similarly occur within C29r (Fox and Scott, 2011). Although it is possible that the variable occurrences of Pu2 within C29r and C29n could indicate increased provinciality across the Western Interior at that time, as has been argued elsewhere, it is also possible that Pu2 simply begins within C29r and extends into C29n (Sprain et al. 2018). Additional high-resolution chronostratigraphic constraints on sections that clearly record the boundary between Pu1 and Pu2 will be needed to resolve this.

CONCLUSIONS

The magnetostratigraphic results reported here indicate that the Corral Bluffs area of the Denver Basin preserves a relatively continuous K–Pg boundary stratigraphic sequence spanning chrons C30n to C28r. These magnetostratigraphic results combined with three palynologically determined K–Pg boundary sites, and two independent $^{206}Pb /^{238}U$ ages for the same ash bed, sampled ~1 km apart, provide one of the very few precisely dated temporal frameworks for a fossil-bearing, continental, latest-Cretaceous to early Paleocene boundary sequence. It is now possible to correlate the fossil localities in this area to contemporaneous sites in the basin, across the region, and around the globe using the GPTS (Gradstein et al., 2012; Ogg, 2012). Our results indicate that the Corral Bluffs Pu2/Pu3 fauna lies within C29n, simi-

lar to what is found in the San Juan Basin of New Mexico, Crazy Mountains Basin of Montana, and Hell Creek area of Montana. Corral Bluffs represents an important candidate for future paleontological investigation due to this new high-resolution temporal framework and its previously noted presence of early Paleocene vertebrates and well-preserved Late Cretaceous and early Paleocene megaflora. Corral Bluffs and Jimmy Camp Creek now represent the most extensive surface exposure in the Denver Basin for which there are chronostratigraphic controls, allowing for the opportunity to interpret fossil collections from this area in the context of K–Pg boundary extinction and recovery.

ACKNOWLEDGMENTS

REFERENCES CITED

Alvarez, L.W., Alvarez, W., Asaro, F., and Michel, H.V., 1980, Extraterrestrial cause for the Cretaceous-Tertiary extinction: Science, v. 208, p. 1,095–1,108, doi:10.1126/science.208.4448.1095.

Archibald, J.D., 1982, A study of Mammalia and geology across the Cretaceous-Tertiary boundary in

Garfield County, Montana: University of California Publications in Geological Sciences, v. 122, *xvi* + 286 p.

Barclay, R.S., Johnson, K.R., Betterton, W.J., and Dilcher, D.L., 2003, Stratigraphy and megaflora of a K-T boundary section in the eastern Denver Basin, Colorado: Rocky Mountain Geology, v. 38, p. 45–71, doi:10.2113/gsrocky.38.1.45.

Bercovici, A., Pearson, D.A., Nichols, D.J., and Wood, J., 2009, Biostratigraphy of selected K/T boundary sections in southwestern North Dakota, USA: Toward a refinement of palynological identification criteria: Cretaceous Research v. 30, p. 632–658, doi:org/10.1016/j.cretres.2008.12.007.

Bercovici, A., Vajda, V., and Sweet, A., 2012, Pollen and spore stratigraphy of the Cretaceous–Paleogene mass-extinction interval in the Northern Hemisphere: Journal of Stratigraphy, v. 36, p. 165–178.

Besse, J., and Courtillot, V., 2003, Correction to "Apparent and true polar wander and the geometry of the geomagnetic field over the last 200 Myr": Journal of Geophysical Research: Solid Earth, v. 108, doi:10.1029/2003JB002684.

Bloemendal, J., King, J.W., Hall, F.R., and Doh, S.-J., 1992, Rock magnetism of Late Neogene and Pleistocene deep-sea sediments: Relationship to sediment source, diagenetic processes, and sediment lithology: Journal of Geophysical Research, v. 97, p. 4,361–4,375, doi:10.1029/91JB03068.

Buckley, G.A., 2018, Magnetostratigraphy of Upper Cretaceous (Lancian) to Middle Paleocene (Tiffanian) strata in the northeastern Crazy Mountains Basin, Montana, U.S.A.: Rocky Mountain Geology, v. 53, p. 59–74, doi:10.24872/rmgjournal.53.2.59.

Butler, R.F., and Lindsay, E.H., 1985, Mineralogy of magnetic minerals and revised magnetic polarity stratigraphy of continental sediments, San Juan Basin, New Mexico: The Journal of Geology, v. 93, p. 535–554.

Clemens, W.A., 2002, Evolution of the mammalian fauna across the Cretaceous-Tertiary boundary in northeastern Montana and other areas of the Western Interior, *in* Hartman, J.H., Johnson, K.R., and Nichols, D.J., eds., The Hell Creek Formation and the Cretaceous-Tertiary boundary in the northern Great Plains: An integrated continental record of the end of the Cretaceous: Boulder, Colorado, Geological Society of America Special Paper 361, p. 217–245, doi:10.1130/0-8137-2361-2.217.

____ 2013, Cf. *Wortmania* from the early Paleocene of Montana and an evaluation of the fossil record of the initial diversification of the Taeniodonta (Mammalia): Canadian Journal of Earth Sciences, v. 50, p. 341–354, doi:10.1139/e2012-055.

Close, R.A., Benson, R.J., Alroy, J., and eight others, 2019, Diversity dynamics of Phanerozoic terrestrial tetrapods at the local-community scale: Nature Ecology & Evolution, v. 3, p. 590–597, doi:10.1038/s41559-019-0811-8.

Clyde, W.C., Ramezani, J., Johnson, K.R., and two others, 2016, Direct high-precision U–Pb geochronology of the end-Cretaceous extinction and calibration of Paleocene astronomical timescales: Earth and Planetary Science Letters, v. 452, p. 272–280, doi:10.1016/j.epsl.2016.07.041.

Clyde, W.C., Wilf, P., Iglesias, A., and 16 others, 2014, New age constraints for the Salamanca Formation and lower Rio Chico Group in the western San Jorge Basin, Patagonia, Argentina: Implications for Cretaceous-Paleogene extinction recovery and land mammal age correlations: Geological Society of America Bulletin, v. 126, p. 289–306, doi:10.1130/B30915.1.

Courtillot, V., Besse, J., Vandamme, D., and three others, 1986, Deccan flood basalts at the Cretaceous/Tertiary boundary?: Earth and Planetary Science Letters, v. 80, p. 361–374, doi:10.1016/0012-821X(86)90118-4.

Cox, A., and Doell, R.R., 1960, Review of paleomagnetism: Geological Society of America Bulletin, v. 71, p. 645–768, doi:10.1130/0016-7606(1960)71[645:ROP]2.0.CO;2.

Dahlberg, E.L., Eberle, J.J., Sertich, J.J.W., and Miller, I.M., 2016, A new earliest Paleocene (Puercan) mammalian fauna from Colorado's Denver Basin, U.S.A.: Rocky Mountain Geology, v. 51, p. 1–22, doi:10.2113/gsrocky.51.1.1.

Davies, T.W., Bell, M.A., Goswami, A., and Halliday, T.J.D., 2017, Completeness of the eutherian mammal fossil record and implications for reconstructing mammal evolution through the Cretaceous/Paleogene mass extinction: Paleobiology, v. 43, p. 521–536, doi:10.1017/pab.2017.20.

Donovan, M.P., Iglesias, A., Wilf, P., and two others, 2018, Diverse plant-insect associations from the Latest Cretaceous and Early Paleocene of Patagonia, Argentina: Ameghiniana, v. 55, p. 303–338, doi:10.5710/AMGH.15.02.2018.3181.

Eberle, J.J., 2003, Puercan mammalian systematics and biostratigraphy in the Denver Formation, Denver Basin, Colorado: Rocky Mountain Geology, v. 38, p. 143–169, doi:10.2113/gsrocky.38.1.143.

Eberle, J.J., and Lillegraven, J.A., 1998, A new important record of earliest Cenozoic mammalian history: Eutheria and paleogeographic/biostratigraphic summaries: Rocky Mountain Geology, v. 33, p. 49–117, doi:10.2113/33.1.49.

Ellis, B., Johnson, K.R., and Dunn, R.E., 2003, Evidence for an in situ early Paleocene rainforest from Castle Rock, Colorado: Rocky Mountain Geology, v. 38, p. 73–100, doi:10.2113/gsrocky.38.1.173.

Erwin, D.H., 2001, Lessons from the past: Biotic recoveries from mass extinctions: Proceedings of the National Academy of Sciences, v. 98, p. 5,399–5,403, doi:10.1073/pnas.091092698.

Farnham, T.M., and Kraus, M.J., 2002, The stratigraphic and climatic significance of Paleogene alluvial paleosols in synorogenic strata of the Denver Basin, Colorado: Rocky Mountain Geology, v. 37, p. 201–213, doi:10.2113/gsrocky.37.2.201.

Fastovsky, D.E., and Bercovici, A., 2016, The Hell Creek Formation and its contribution to the Cretaceous–Paleogene extinction: A short primer: Cretaceous

Anthony J. Fuentes, William C. Clyde, Ken Weissenburger, Antoine Bercovici, Tyler R. Lyson, Ian M. Miller, Jahandar Ramezani, Vincent Isakson, Mark D. Schmitz, and Kirk R. Johnson

Research, v. 57, p. 368–390, doi:10.1016/j.cre-tres.2015.07.007.

Fisher, R.A., 1953, Dispersion on a sphere: Proceedings of the Royal Society of London Series A:. Mathematical and Physical Sciences, v. 217, p. 295–305, doi:10.1098/rspa.1953.0064.

Fox, R.C., and Scott, C.S., 2011, A new, early Puercan (earliest Paleocene) species of *Purgatorius* (Plesiadapiformes, Primates) from Saskatchewan, Canada: Journal of Paleontology, v. 85, p. 537–548, doi:10.1666/10-059.1.

Gradstein, F.M., Ogg, J.G., Schmitz, M.D., and Ogg, G., 2012, The geologic time scale 2012 (first edition): Boston, Massachusetts, Elsevier, 1,176 p.

Grossnickle, D.M., and Newham, E., 2016, Therian mammals experience an ecomorphological radiation during the Late Cretaceous and selective extinction at the K–Pg boundary: Proceedings of the Royal Society B: Biological Sciences, v. 283, doi:10.1098/rspb.2016.0256.

Håkansson, E., and Thomsen, E., 1999, Benthic extinction and recovery patterns at the K/T boundary in shallow water carbonates, Denmark: Palaeogeography, Palaeoclimatology, Palaeoecology, v. 154, p. 67–85, doi:10.1016/S0031-0182(99)00087-5.

Halliday, T.J.D., Upchurch, P., and Goswami, A., 2017, Resolving the relationships of Paleocene placental mammals: Paleocene mammal phylogeny: Biological Reviews, v. 92, p. 521–550, doi:10.1111/brv.12242.

Heslop, D., and Roberts, A.P., 2018, Revisiting the paleomagnetic reversal test: A Bayesian hypothesis testing framework for a common mean direction: Journal of Geophysical Research: Solid Earth, v. 123, p. 7,225–7,236, doi:10.1029/2018JB016081.

Hicks, J.F., Johnson, K.R., Obradovich, J.D., and two others, 2003, Magnetostratigraphy of Upper Cretaceous (Maastrichtian) to lower Eocene strata of the Denver Basin, Colorado: Rocky Mountain Geology, v. 38, p. 1–27, doi:10.2113/gsrocky.38.1.1.

Hull, P.M., and Norris, R.D., 2011, Diverse patterns of ocean export productivity change across the Cretaceous-Paleogene boundary: New insights from biogenic barium: Paleoceanography, v. 26, PA3205, doi:10.1029/2010PA002082.

Hull, P.M., Darroch, S.A.F., and Erwin, D.H., 2015, Rarity in mass extinctions and the future of ecosystems: Nature, v. 528, p. 345–351, doi:10.1038/nature16160.

Hunter, J.P., and Archibald, J.D., 2002, Mammals from the end of the age of dinosaurs in North Dakota and southeastern Montana, with a reappraisal of geographic differentiation among Lancian mammals, *in* Hartman, J.H., Johnson, K.R., and Nichols, D.J., eds., The Hell Creek Formation and the Cretaceous-Tertiary boundary in the northern Great Plains: An integrated continental record of the end of the Cretaceous: Boulder, Colorado, Geological Society of America Special Paper 361, p. 191–216, doi:10.1130/0-8137-2361-2.191.

Hunter, J.P., Hartman, J.H., and Krause, D.W., 1997, Mammals and mollusks across the Cretaceous-Tertiary boundary from Makoshika State Park and vicinity (Williston Basin), Montana: Laramie, Wyoming,

University of Wyoming, Contributions to Geology, v. 32, p. 61–114.

Iglesias, A., Wilf, P., Johnson, K.R., and four others, 2007, A Paleocene lowland macroflora from Patagonia reveals significantly greater richness than North American analogs: Geology, v. 35, p. 947–950, doi:10.1130/G23889A.1.

Jablonski, D., 1998, Geographic variation in the molluscan recovery from the end-Cretaceous extinction: Science, v. 279, p. 1,327–1,330, doi:10.1126/science.279.5355.1327.

Johnson, K.R., 2002, Megaflora of the Hell Creek and lower Fort Union Formations in the western Dakotas: Vegetational response to climate change, the Cretaceous-Tertiary boundary event, and rapid marine transgression, *in* Hartman, J.H., Johnson, K.R., and Nichols, D.J., eds., The Hell Creek Formation and the Cretaceous-Tertiary boundary in the northern Great Plains: An integrated continental record of the end of the Cretaceous: Boulder, Colorado, Geological Society of America Special Paper 361, p. 329–391, doi:10.1130/0-8137-2361-2.329.

Johnson, K.R., and Ellis, B., 2002, A tropical rainforest in Colorado 1.4 million years after the Cretaceous-Tertiary boundary: Science, v. 296, p. 2,379–2,383, doi:10.1126/science.1072102.

Johnson, K.R., Reynolds, M.L., Werth, K.W., and Thomasson, J.R., 2003, Overview of the Late Cretaceous, early Paleocene, and early Eocene megafloras of the Denver Basin, Colorado: Rocky Mountain Geology, v. 38, p. 101–120, doi:10.2113/gsrocky.38.1.101.

Kelley, S.A., 2002, Unroofing of the southern Front Range, Colorado: A view from the Denver Basin: Rocky Mountain Geology, v. 37, p. 189–200, doi:10.2113/gsrocky.37.2.189.

Kiessling, W., and Baron-Szabo, R.C., 2004, Extinction and recovery patterns of scleractinian corals at the Cretaceous-Tertiary boundary: Palaeogeography, Palaeoclimatology, Palaeoecology, v. 214, p. 195–223, doi:10.1016/j.palaeo.2004.05.025.

Kirschvink, J.L., 1980, The least-squares line and plane and the analysis of palaeomagnetic data: Geophysical Journal International, v. 62, p. 699–718, doi:10.1111/j.1365-246X.1980.tb02601.x.

LeCain, R., Clyde, W.C., Wilson, G.P., and Riedel, J., 2014, Magnetostratigraphy of the Hell Creek and lower Fort Union Formations in northeastern Montana, *in* Wilson, G.P., Clemens, W.A., Horner, J.R., and Hartman, J.H., eds., Through the end of the Cretaceous in the type locality of the Hell Creek Formation in Montana and adjacent areas: Boulder, Colorado, Geological Society of America Special Paper 503, p. 137–147, doi:10.1130/2014.2503(04).

Lillegraven, J.A., and Eberle, J.J., 1999, Vertebrate faunal changes through Lancian and Puercan time in southern Wyoming: Journal of Paleontology, v. 73, p. 691–710.

Lofgren, D.L., Lillegraven, J.A., Clemens, W.A., and two others, 2004, Paleocene biochronology: The Puercan

through Clarkforkian Land Mammal Ages, *in* Woodburne, M.O., ed., Late Cretaceous and Cenozoic mammals of North America: Biostratigraphy and geochronology: New York, New York, Columbia University Press, p. 43–105.

Longrich, N.R., Scriberas, J., and Wills, M.A., 2016, Severe extinction and rapid recovery of mammals across the Cretaceous–Palaeogene boundary, and the effects of rarity on patterns of extinction and recovery: Journal of Evolutionary Biology, v. 29, p. 1,495–1,512, doi:10.1111/jeb.12882.

Lowery, C.M., Bralower, T.J., Owens, J.D., and 35 others, 2018, Rapid recovery of life at ground zero of the end-Cretaceous mass extinction: Nature, v. 558, p. 288–291, doi:10.1038/s41586-018-0163-6.

Lowrie, W., 1990, Identification of ferromagnetic minerals in a rock by coercivity and unblocking temperature properties: Geophysical Research Letters, v. 17, p. 159–162, doi:10.1029/GL017i002p00159.

Lurcock, P.C., and Wilson, G.S., 2012, PuffinPlot: A versatile, user-friendly program for paleomagnetic analysis: Geochemistry, Geophysics, Geosystems, v. 13, Q06Z45, doi:10.1029/2012GC004098.

Maxbauer, D.P., Feinberg, J.M., and Fox, D.L., 2016, Magnetic mineral assemblages in soils and paleosols as the basis for paleoprecipitation proxies: A review of magnetic methods and challenges: Earth-Science Reviews, v. 155, p. 28–48, doi:10.1016/j.earscirev.2016.01.014.

McFadden, P.L., and McElhinny, M.W., 1988, The combined analysis of remagnetization circles and direct observations in palaeomagnetism: Earth and Planetary Science Letters, v. 87, p. 161–172, doi:10.1016/0012-821X(88)90072-6.

McIver, E.E., 1999, Paleobotanical evidence for ecosystem disruption at the Cretaceous–Tertiary boundary from Wood Mountain, Saskatchewan, Canada: Canadian Journal of Earth Sciences, v. 36, p. 775–789, doi:10.1139/e97-112.

Middleton, M.D., 1983, Early Paleocene vertebrates of the Denver Basin, Colorado [Ph.D. dissert.]: Boulder, Colorado, University of Colorado, 404 p.

Middleton, M.D., and Dewar, E.W., 2004, New mammals from the early Paleocene Littleton fauna (Denver Formation, Colorado): New Mexico Museum of Natural History and Science Bulletin, v. 26, p. 59–80.

Mizukami, T., Kaiho, K., and Oba, M., 2013, Significant changes in land vegetation and oceanic redox across the Cretaceous/Paleogene boundary: Palaeogeography, Palaeoclimatology, Palaeoecology, v. 369, p. 41–47, doi:10.1016/j.palaeo.2012.09.020.

Nichols, D.J., 1994, A revised palynostratigraphic zonation of the nonmarine Upper Cretaceous, Rocky Mountain region, United States, *in* Caputo, M.V., Peterson, J.A., and Franczyk, K.J., eds., Mesozoic systems of the Rocky Mountain region, USA: Denver, Colorado, Society of Economic Paleontologists and Mineralogists, Rocky Mountain Section, p. 503–522.

Nichols, D.J., and Fleming, R.F., 2002, Palynology and palynostratigraphy of Maastrichtian, Paleocene, and Eocene strata in the Denver Basin, Colorado: Rocky Mountain Geology, v. 37, p. 135–163, doi:10.2113/gsrocky.37.2.135.

Nichols, D.J., Hartman, J., and Johnson, K., 2002, Palynology and palynostratigraphy of the Hell Creek Formation in North Dakota: A microfossil record of plants at the end of Cretaceous time, *in* Hartman, J.H., Johnson, K.R., and Nichols, D.J., eds., The Hell Creek Formation and the Cretaceous–Tertiary boundary in the northern Great Plains: An integrated continental record of the end of the Cretaceous: Boulder, Colorado: Geological Society of America Special Paper 361, p. 393–456, doi:10.1130/0-8137-2361-2.393.

Nichols, D.J., and Johnson, K.R., 2002, Palynology and microstratigraphy of Cretaceous–Tertiary boundary sections in southwestern North Dakota, *in* Hartman, J.H., Johnson, K.R., and Nichols, D.J., eds., The Hell Creek Formation and the Cretaceous–Tertiary boundary in the northern Great Plains: An integrated continental record of the end of the Cretaceous: Boulder, Colorado, Geological Society of America Special Paper 361, p. 95–143, doi:10.1130/0-8137-2361-2.95.

___ 2008, Plants and the K–T boundary: Cambridge, United Kingdom, Cambridge University Press, 292 p., doi:10.1017/CBO9780511535536.

Ogg, J.G., 2012, Geomagnetic polarity time scale, *in* Gradstein, F.M., Ogg, J.G., Schmitz, M.D., and Ogg, G.M. eds., The Geologic Time Scale 2012 (first edition): Boston, Massachusetts, Elsevier, p. 85–113, doi:10.1016/B978-0-444-59425-9.00005-6.

O'Leary, M.A., Bloch, J.I., Flynn, J.J., and 20 others, 2013, The placental mammal ancestor and the post-K–Pg radiation of placentals: Science, v. 339, p. 662–667, doi:10.1126/science.1229237.

Özdemir, Ö., and Banerjee, S.K., 1984, High temperature stability of maghemite (γ-Fe$_2$O$_3$): Geophysical Research Letters, v. 11, p. 161–164, doi:10.1029/GL011i003p00161.

Paleobiology Database, 2019, Welcome to PBDB navigator!: *at* https://paleobiodb.org/navigator/#/fc195dcd (accessed May 2019).

Peppe, D.J., Heizler, M.T., Williamson, T.E., and four others, 2013, New age constraints on the Late Cretaceous through Early Paleogene rocks in the San Juan Basin, New Mexico: Geological Society of America Abstracts with Programs, v. 45, no. 7, p. 290.

Peppe, D.J., Evans, D.A.D., and Smirnov, A.V., 2009, Magnetostratigraphy of the Ludlow Member of the Fort Union Formation (Lower Paleocene) in the Williston Basin, North Dakota: Geological Society of America Bulletin, v. 121, p. 65–79, doi:10.1130/B26353.1.

Raynolds, R.G., 2002, Upper Cretaceous and Tertiary stratigraphy of the Denver Basin, Colorado: Rocky Mountain Geology, v. 37, p. 111–134, doi:10.2113/gsrocky.37.2.111.

Raynolds, R.G., and Johnson, K.R., 2003, Synopsis of the stratigraphy and paleontology of the uppermost Cretaceous and lower Tertiary strata in the Denver Basin, Colorado: Rocky Mountain Geology, v. 38, p. 171–181, doi:10.2113/gsrocky.38.1.171.

Raynolds, R.G.H., Johnson, K.R., Arnold, L.R., and eight others, 2001, The Kiowa core, a continuous drill core through the Denver Basin bedrock aquifers at Kiowa, Elbert County, Colorado: U.S. Geological Survey Open-File Report 2001-185, 127 p., doi:10.3133/ofr01185.

Robson, S.G., and Banta, E.R., 1993, Data from core analyses, aquifer testing, and geophysical logging of Denver Basin bedrock aquifers at Castle Pines, Colorado: U.S. Geological Survey Open-File Report 93-442, *iv* + 94 p., doi:org/10.3133/ofr93442.

Schoene, B., Eddy, M.P., Samperton, K.M., and four others, 2019, U-Pb constraints on pulsed eruption of the Deccan Traps across the end-Cretaceous mass extinction: Science, v. 363, p. 862–866, doi:10.1126/science.aau2422.

Schoene, B., Samperton, K.M., Eddy, M.P., and five others, 2015, U-Pb geochronology of the Deccan Traps and relation to the end-Cretaceous mass extinction: Science, v. 347, p. 182–184, doi:10.1126/science.aaa0118.

Schulte, P., Alegret, L., Arenillas, I., and 38 others, 2010, The Chicxulub asteroid impact and mass extinction at the Cretaceous-Paleogene boundary: Science, v. 327, p. 1,214–1,218, doi:10.1126/science.1177265.

Smith, S.M., Sprain, C.J., Clemens, W.A., and three others, 2018, Early mammalian recovery after the end-Cretaceous mass extinction: A high-resolution view from McGuire Creek area, Montana, USA: Geological Society of America Bulletin, v. 130, p. 2,000–2,014, doi:10.1130/B31926.1.

Sprain, C.J., Feinberg, J.M., Renne, P.R., and Jackson, M., 2016, Importance of titanohematite in detrital remanent magnetizations of strata spanning the Cretaceous-Paleogene boundary, Hell Creek region, Montana: Geochemistry, Geophysics, Geosystems, v. 17, p. 660–678, doi:10.1002/2015GC006191.

Sprain, C.J., Renne, P.R., Clemens, W.A., and Wilson, G.P., 2018, Calibration of chron C29r: New high-precision geochronologic and paleomagnetic constraints from the Hell Creek region, Montana: Geological Society of America Bulletin, v. 130, p. 1,615–1,644, doi:10.1130/B31890.1.

Sprain, C.J., Renne, P.R., Vanderkluysen, L., and three others, 2019, The eruptive tempo of Deccan volcanism in relation to the Cretaceous-Paleogene boundary: Science, v. 363, p. 866–870, doi:10.1126/science.aav1446.

Sprain, C.J., Renne, P.R., Wilson, G.P., and Clemens, W.A., 2015, High-resolution chronostratigraphy of the terrestrial Cretaceous-Paleogene transition and recovery interval in the Hell Creek region, Montana: Geological Society of America Bulletin, v. 127, p. 393–409, doi:10.1130/B31076.1.

Stober, J.C., and Thompson, R., 1979, Magnetic remanence acquisition in Finnish lake sediments: Geophysical Journal International, v. 57, p. 727–739, doi:10.1111/j.1365-246X.1979.tb06786.x.

Sweet, A.R., and Braman, D.R.,1992, The K–T boundary and the contiguous strata in western Canada: Interactions between paleoenvironments and paly-nological assemblages: Cretaceous Research, v. 13, p. 31–79, doi:10.1016/0195-6671(92)90027-N.

____ 2001, Cretaceous-Tertiary palynofloral perturbations and extinctions within the *Aquilapollenites* Phytogeographic Province: Canadian Journal of Earth Sciences, v. 38, p. 249–269, doi:10.1139/e00-024.

Sweet, A.R., Braman, D.R., and Lerbekmo, J.F., 1990, Palynofloral response to the K/T boundary events; A transitory interruption within a dynamic system, *in* Sharpton, V.L., and Ward, P.D., eds., Global catastrophes in Earth history; An interdisciplinary conference on impacts, volcanism, and mass mortality: Boulder, Colorado, Geological Society of America Special Paper 247, p. 457–469, doi:10.1130/SPE247-p457.

____1999, Sequential palynological changes across the composite Cretaceous-Tertiary (K-T) boundary claystone and contiguous strata, western Canada and Montana, U.S.A. Canadian Journal of Earth Sciences v. 36, p. 743–768, doi:10.1139/e98-061.

Swisher, C.C., III, Dingus, L., and Butler, R.F., 1993, $^{40}Ar/^{39}Ar$ dating and magnetostratigraphic correlation of the terrestrial Cretaceous–Paleogene boundary and Puercan Mammal Age, Hell Creek – Tullock formations, eastern Montana: Canadian Journal of Earth Sciences, v. 30, p. 1,981–1,996, doi:10.1139/e93-174.

Tauxe, L, Banerjee, S.K., Butler, R.F., and Van der Voo, R., 2018, Essentials of paleomagnetism (fifth web edition): Berkeley, California, University of California Press: *at* https://earthref.org/MagIC/books/Tauxe/Essentials/.

Torsvik, T.H., Van der Voo, R., Preeden, U., and 10 others, 2012, Phanerozoic polar wander, palaeogeography and dynamics: Earth-Science Reviews , v. 114, p. 325–368, doi:10.1016/j.earscirev.2012.06.007.

Vajda, V., and Bercovici, A., 2014, The global vegetation pattern across the Cretaceous–Paleogene mass extinction interval: A template for other extinction events: Global and Planetary Change, v. 122, p. 29–49, doi:10.1016/j.gloplacha.2014.07.014.

Vajda, V., and McLoughlin, S., 2007, Extinction and recovery patterns of the vegetation across the Cretaceous–Palaeogene boundary — a tool for unravelling the causes of the end-Permian mass-extinction: Review of Palaeobotany and Palynology, v. 144, p. 99–112, doi:10.1016/j.revpalbo.2005.09.007.

van Velzen, A.J., and Dekkers, M.J., 1999, Low-temperature oxidation of magnetite in Loess-Paleosol sequences: a correction of rock magnetic parameters: Studia Geophysica et Geodaetica, v. 43, p. 357–375, doi:10.1023/A:1023278901491.

Watson, G.S., 1956, A test for randomness of directions: Geophysical Journal International, v. 7, p. 160–161, doi:10.1111/j.1365-246X.1956.tb05561.x.

Williamson, T.E., 1996, The beginning of the age of mammals in the San Juan Basin, New Mexico: Biostratigraphy and evolution of Paleocene mammals of the Nacimiento Formation: New Mexico Museum of Natural History and Science Bulletin 8, 141 p.

Williamson, T.E., Brusatte, S.L., Carr, T.D., and two others, 2012, The phylogeny and evolution of Cretaceous–

Palaeogene metatherians: cladistic analysis and description of new early Palaeocene specimens from the Nacimiento Formation, New Mexico: Journal of Systematic Palaeontology, v. 10, p. 625–651, doi:10.1080/14772019.2011.631592.

Wilson, G.P., 2013, Mammals across the K/Pg boundary in northeastern Montana, U.S.A.: dental morphology and body-size patterns reveal extinction selectivity and immigrant-fueled ecospace filling: Paleobiology, v. 39, p. 429–469, doi:10.1666/12041.

___ 2014, Mammalian extinction, survival, and recovery dynamics across the Cretaceous-Paleogene boundary in northeastern Montana, USA, *in* Wilson, G.P., Clemens, W.A., Horner, J.R., and Hartman, J.H., eds., Through the end of the Cretaceous in the type locality of the Hell Creek Formation in Montana and adjacent areas: Boulder, Colorado, Geological Society of America Special Paper 503, p. 365–392, doi:10.1130/2014.2503(15).

Wilson, M.D., 2002, Petrographic provenance analysis of Kiowa Core sandstone samples, Denver Basin, Colorado: Rocky Mountain Geology, v. 37, p. 173–187, doi:10.2113/gsrocky.37.2.173.

Witts, J.D., Whittle, R.J., Wignall, P.B., and four others, 2016, Macrofossil evidence for a rapid and severe Cretaceous–Paleogene mass extinction in Antarctica: Nature Communications, v. 7, article 11738, doi:10.1038/ncomms11738.

Zaiss, J., Ravizza, G., Goderis, S., and three others, 2014, A complete Os excursion across a terrestrial Cretaceous–Paleogene boundary at the West Bijou Site, Colorado, with evidence for recent open system behavior: Chemical Geology, v. 385, p. 7–16, doi:10.1016/j.chemgeo.2014.07.010.

ASSOCIATE EDITOR: JAELYN J. EBERLE